

**SECONDARY DENDRITE ARM SPACING
DETERMINATION IN Al-Si CASTING ALLOYS
BY CONDUCTIVITY MEASUREMENTS**

by

A. CHARBONNIER

A Thesis submitted to the Faculty of Graduate Studies and Research
in partial fulfillment of the requirements for degree of
Master of Engineering

Departement of Mining & Metallurgical Engineering
McGill University, Montréal, CANADA

February 1992.

© A. Charbonnier 1992

ACKNOWLEDGEMENTS

I would like to express my deep gratitude to my thesis supervisor, Professor J.E. Gruzleski for his guidance, constant support, and especially for his unequalled patience throughout the preparation of this work.

I am very grateful to my colleagues and friends Dr. H. Mülazimoglu, A. Aliravci, F. Paray, N. Tenekedjiev, W. Wang, W. La Orchan and T. Joenes for their recommendations and technical collaboration.

Sincere acknowledgements are also extended to R. Paquette for his help with the experiments.

ABSTRACT

Al-Si-Mg alloys containing 7% silicon are the most widely used aluminum foundry alloys owing to their good mechanical properties and excellent castability. Nevertheless, design engineers traditionally apply a design casting factor when designing cast components to ensure that proper strength will be obtained in spite of the recent emergence of techniques of control of the molten alloy quality on which depend, afterwards, the mechanical properties of the castings.

In this study, the feasibility of using electrical conductivity to non destructively predict secondary dendrite arm spacing was investigated on both as-cast and heat treated alloys. In the as-cast condition, conductivity decreases linearly with increasing DAS from 30 μm , while, below 30 μm , conductivity readings are influenced by alloying elements retained in solid solution due to the fast solid state cooling rates. Conductivity changes with DAS are more important when the silicon morphology is finer i.e. the alloy modified. After heat treatment, the DAS-conductivity relationships become linear as a result of the homogenisation of the aluminum matrix, but the slopes of the lines are small and the accuracy of DAS determination does not extend below 15 μm . Conductivity is also greatly influenced by the degree of precipitation achieved during artificial aging so that the determination of DAS by conductivity measurement is best used after quenching (T4 condition).

RESUME

Les alliages Al-Si-Mg à 7% de silicium sont les plus largement utilisés en fonderie en raison de leurs bonnes caractéristiques mécaniques et leurs excellentes propriétés de fonderie. Néanmoins, les ingénieurs d'études appliquent régulièrement un coefficient de fonderie lors de la conception de pièces moulées en dépit du récent développement de méthodes de contrôle de la qualité du métal liquide dont dépendent les caractéristiques mécaniques ultérieures des pièces coulées.

Cette étude a porté sur la possibilité d'utiliser la conductivité électrique pour déterminer l'espacement des bras de dendrite secondaires ou DAS (une caractéristique métallurgique dépendant de la vitesse de solidification et qui a une influence significative sur les caractéristiques mécaniques) pour des alliages traités thermiquement ou non. A l'état non traité, la conductivité décroît linéairement à partir d'un DAS supérieur à 30 μm , alors qu'au dessous de 30 μm , les valeurs sont influencées par la sursaturation en éléments d'alliage de la solution solide d'aluminium due à une vitesse de refroidissement à l'état solide élevée. Les variations de conductivité avec le DAS sont d'autant plus importantes que le silicium eutectique est fin c'est à dire que l'alliage est modifié. Après traitement thermique, les courbes conductivité = f (DAS) deviennent linéaires du fait de l'homogénéisation de la matrice d'aluminium, mais leurs pentes restent faibles de sorte que la précision dans la détermination du DAS reste supérieure à 15 μm . La conductivité est également fortement influencée par le degré de précipitation obtenu par revenu ce qui implique que la détermination du DAS doit être faite juste après trempe (état T4).

CONTENTS

<u>CHAPTER 1 - INTRODUCTION</u>	Page	1
1. <u>Al-Si-Mg casting alloys</u>	Page	1
1.1 Effect of alloying elements and impurities	Page	1
1.11 Silicon	Page	1
1.12 Magnesium	Page	3
1.13 Iron	Page	5
1.14 Titanium	Page	5
1.2 A356 and A357 casting alloys	Page	6
1.21 Composition and properties	Page	6
2. <u>Factors influencing mechanical properties</u>	Page	7
2.1 Iron content	Page	7
2.2 Modification	Page	7
2.3 Porosity	Page	8
2.4 Dendrite arm spacing	Page	10
3. <u>Aim of the present research</u>	Page	13
<u>CHAPTER 2 - THEORETICAL BACKGROUND AND LITERATURE REVIEW</u>	Page	14
1. <u>Theory of electrical conductivity/resistivity</u>	Page	14
1.1 Pure metals	Page	14
1.2 Alloys	Page	17
1.21 Solid solutions	Page	17
1.22 Multiphase alloys	Page	19
2. <u>Modification of eutectic silicon</u>	Page	20
2.1 Nucleation of silicon	Page	21
2.2 Growth of eutectic silicon particles	Page	22

3. <u>Dendrite arm spacing</u>	Page	25
3.1 Dendritic solidification	Page	25
3.2 Importance of dendrite arm spacing	Page	28
4. <u>Application of electrical conductivity in metallurgy of Al-Si casting alloys</u>	Page	30
4.1 Assessment of the degree of modification	Page	30
4.2 Heat treatment	Page	33
4.3 Application to Al-Si-Mg alloys	Page	34
4.4 Determination of dendrite arm spacing	Page	36
<u>CHAPTER 3 - EXPERIMENTAL PROCEDURE</u>	Page	37
1. <u>Design of the casting</u>	Page	38
2. <u>Materials</u>	Page	40
2.1 Moulding	Page	40
2.2 Alloys	Page	40
3. <u>Melt processing</u>	Page	42
3.1 Melting and alloying	Page	42
3.2 Degassing	Page	43
3.3 Melt quality control	Page	44
3.4 Casting	Page	45
3.5 Heat treatment	Page	46
4. <u>Sample characterisation</u>	Page	47
4.1 Electrical conductivity measurement	Page	47
4.2 Metallography	Page	52
4.3 Determination of the degree of modification	Page	53
4.4 Dendrite arm spacing	Page	56
4.5 Spectrochemical analysis	Page	58

<u>CHAPTER 4 - RESULTS AND DISCUSSION</u>	Page	59
1. <u>As cast conductivity</u>	Page	62
1.1 Synthetic alloys	Page	62
1.2 A356 alloys	Page	65
1.3 Calculation of polynomial model fitting		
the experimental results	Page	68
2. <u>Influence of a precipitation treatment</u>	Page	72
2.1 Synthetic alloys	Page	73
2.2 A356 alloys	Page	74
3. <u>Heat treatment</u>	Page	76
3.1 Al-Si synthetic alloys	Page	77
3.11 Unmodified alloys	Page	77
3.12 Modified synthetic alloys	Page	79
3.2 A356 alloys	Page	80
3.21 Unmodified alloy	Page	80
3.22 Modified alloy	Page	83
4. <u>Discussion</u>	Page	84
4.1 Unmodified Al-Si alloy	Page	88
4.2 Modified Al-Si alloy	Page	88
4.3 Unmodified A356	Page	89
4.4 A356 modified alloy	Page	91
4.5 Influence of precipitation	Page	91
4.6 Potential Industrial Application	Page	92
<u>CONCLUSION</u>	Page	94
<u>BIBLIOGRAPHY</u>	Page	95

List of Figures

- Figure 1.1 Al-Si phase diagram
- Figure 1.2 Microstructure of an as-cast Al-Si-Mg alloy. Mag. X 560
- Figure 1.3 Influence of the magnesium content on mechanical properties
- Figure 1.4 Microstructure of as cast A356 alloy exhibiting microporosity as black areas. Mag. X20
- Figure 1.5 Microstructures of modified and unmodified A356 alloy
- Figure 1.6 Microstructures of as-cast A356 alloy with different DAS
- Figure 2.1 Solid-liquid interfaces in Al-Si eutectic alloys
- Figure 2.2 The TPPE growth mechanism
- Figure 2.3 Definition of the Dendrite Arm Spacing
- Figure 2.4 Constitutional undercooling
- Figure 2.5 Mechanisms of dendrite arm coarsening
- Figure 2.6 Tensile properties variation with DAS of 356.T6 alloy
- Figure 2.7 Conductivity variation with silicon content for modified and unmodified A356 alloy
- Figure 2.8 Mechanism of electron scattering at Al-Si interface
- Figure 2.9 Stages of conductivity changes during solution treatment
- Figure 2.10 Variation of conductivity with DAS for modified and unmodified A356 alloy
- Figure 3.1 Step casting
- Figure 3.2 Aluminum chill
- Figure 3.3 Degassing technique
- Figure 3.4 Sand moulds after casting
- Figure 3.5 K.J. Law eddy current tester
- Figure 3.6 Principle of eddy current technique
- Figure 3.7 Conductivity readings on as cast and machined surfaces

- Figure 3.8 Variation of conductivity with sample thickness
- Figure 3.9 Location of the metallographic samples
- Figure 3.10 Modification rating system
- Figure 3.11 DAS measurement technique
- Figure 4.1 Micrographs showing the range of DAS covered
- Figure 4.2 Conductivity vs DAS plots for Al-Si binary alloy
- Figure 4.3 Conductivity vs DAS plots for A356 alloy
- Figure 4.4 Polynomial model response surface
- Figure 4.5 Polynomial model contour plot
- Figure 4.6 Conductivity vs DAS plot for Al-Si binary alloy as-cast and after precipitation treatment
- Figure 4.7 Conductivity vs DAS plot for A356 alloy as-cast and after precipitation treatment
- Figure 4.8 Conductivity vs DAS plots for unmodified Al-Si alloy (As cast, T4 & T6 conditions)
- Figure 4.9 Conductivity vs DAS plots for modified Al-Si alloy (As cast, T4 & T6 conditions)
- Figure 4.10 Conductivity vs DAS plots for unmodified A356 alloy (As cast, T4 & T6 conditions)
- Figure 4.11 Micrographs of as cast unmodified Al-Si and A356 alloys. Mag.X150
- Figure 4.12 Conductivity vs DAS plots for modified A356 alloy (As cast, T4 & T6 conditions)
- Figure 4.13 Micrographs of as cast and T6 unmodified Al-Si alloy at two different DAS. Mag.X 500
- Figure 4.14 Micrographs of as cast and T6 modified A356 alloy at two different DAS. Mag X 500
- Figure 4.15 Micrographs of as cast and T6 unmodified A356 alloy at two different DAS Mag X 500
- Figure 4.16 Conductivity vs DAS plots for A356 modified alloy. Influence of overaging

List of Tables

Table 1.1 : Composition of A356 and A357 alloys

Table 1.2 : Mechanical properties of A356 and A357 alloys (T6)

Table 1.3 : Mechanical properties of unmodified and modified A356 and A357 alloys

Table 2.1 : Effect of alloying elements on the resistivity of pure aluminium

Table 3.1 : Chemical compositions of the primary ingots and master alloys used

Table 3.2 : Chemistry of the melts

Table 4.1 : Coefficients of the polynomial model

CHAPTER 1

INTRODUCTION

Al-Si-Mg alloys have found many applications in the aerospace and automotive industries owing to their low densities (2.6 to 2.8 g/cm³). These alloys possess good tensile and fatigue properties, good corrosion resistance, and have a good castability. They can be cast by almost all conventional casting methods such as sand, permanent mould, investment and high pressure die casting.

1. Al-Si-Mg CASTING ALLOYS

1.1 Effect of the alloying elements and impurities

1.11 Silicon

The aluminum-silicon system comprises an eutectic reaction at 577°C and 11.7% Si as seen on the phase diagram in Figure 1.1.

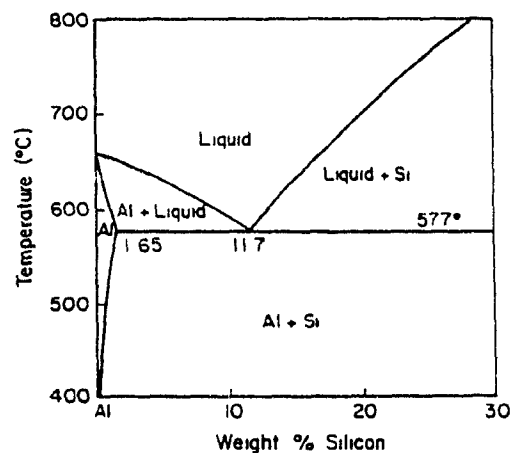


Figure 1.1 : Al-Si phase diagram

Silicon has a limited solubility in solid aluminum, and at concentrations exceeding 1.6%, hard and discontinuous particles of pure silicon form through the eutectic reaction (Figure 1.2).

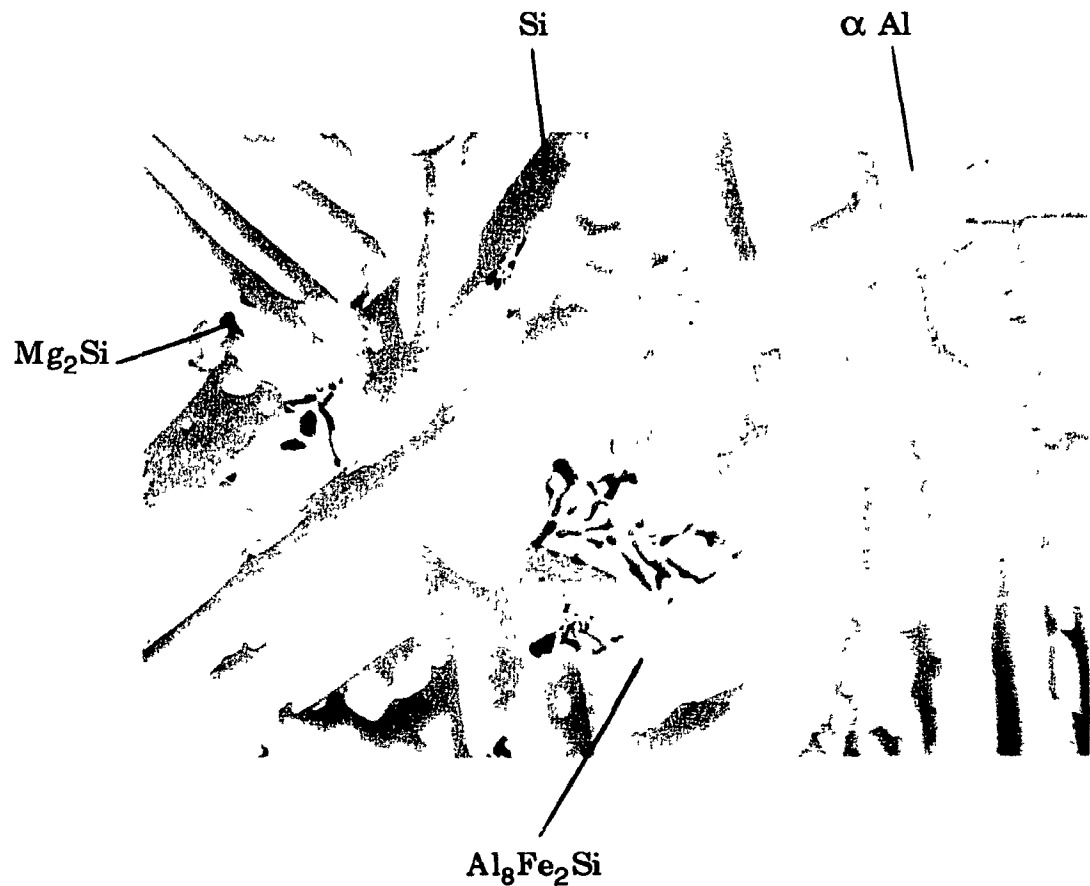


Figure 1.2 : Microstructure of an as cast Al Si Mg alloy - Mg = 0.6 %. Mag. X 560

Silicon, by reducing the interval of solidification, also imparts excellent castability and resistance to hot tearing to the alloys [1]. Both tensile strength and yield strength increase with silicon additions of up to about 7% while elongation decreases.

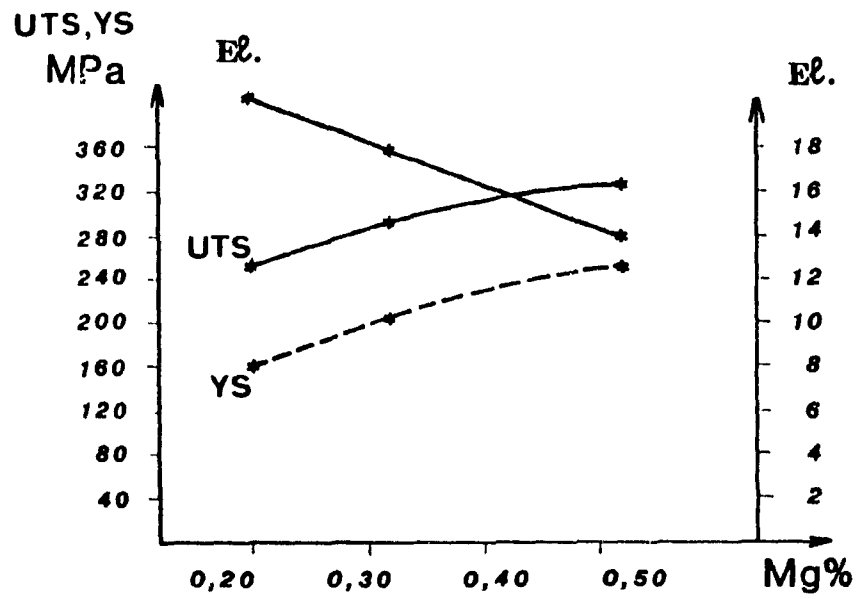
At concentrations greater than 7%, the rate of increase in tensile strength decreases. Besides concentration, the mechanical properties of the cast component are determined by the morphology of the silicon particles in the matrix [2]. Optimum properties are achieved with small and spherical particles. The best compromise between tensile properties and castability is obtained at 7% silicon. The most common foundry alloys are therefore in this composition range.

1.12 Magnesium

Magnesium is added to Al-Si alloys for heat treatment purposes. Magnesium combines with silicon to form the age-hardening compound Mg_2Si (Figure 1.2) which, when finely precipitated from solid solution during heat treatment, is responsible for the improvement in mechanical strength [3]. In the as cast state, magnesium is mostly present as Mg_2Si particles of Chinese script morphology.

Depending on the cooling rate after solidification, some magnesium is also retained in solid solution and promotes a slight solution strengthening of the alloy. Magnesium content is typically less than about 0.75%, because higher levels impair fluidity and feeding [4]. In addition, some Mg_2Si particles remain undissolved after heat treatment when the magnesium concentration exceeds 0.75%, which reduces ductility (Figure 1.3).

Permanent mould



Sand mould

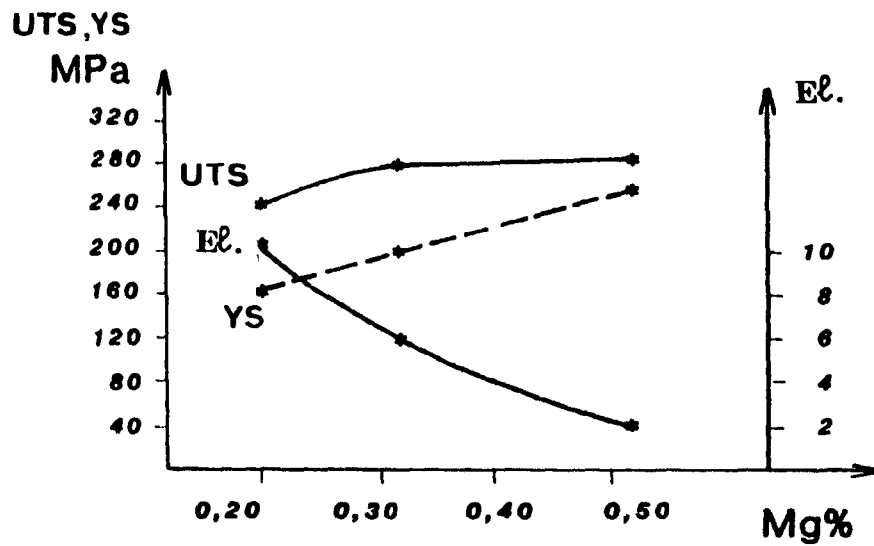


Figure 1.3 : Influence of the magnesium content on mechanical properties [9]

1.13 Iron

Iron is present in aluminum alloys as an impurity at concentrations not exceeding 1% [5]. It has a limited solubility in aluminum and combines with silicon and aluminum to form brittle intermetallic compounds (Figure 1.2) which greatly impair ductility, [6]. In addition, the shape and number of iron bearing compounds are not changed by heat treatment [7]. For premium quality casting production, the iron content is kept at a minimum lower than 0.2%.

1.14 Titanium

Titanium is added on purpose to aluminum alloys for grain refinement usually in the form of master alloys. It forms Al_3Ti compounds with liquid aluminum which are known to serve as a nucleant for aluminum. Titanium levels range from 0.05% to 0.2%.

1.2 A356 & A357 casting alloys

1.21 Compositions and Properties

The most common casting alloys in the Al-Si-Mg family are A356 and A357 whose compositions are listed in Table 1.1 [8]. These alloys constitute the best compromise between mechanical properties and casting characteristics. Table 1.2 [9] lists the tensile properties of A356 and A357 measured on sand and permanent mould cast test bars after heat treatment. A356 and A357 alloys are seldom used in the as-cast state except in Europe where wheels are cast in A356 by the low pressure process. In general, desired mechanical strength on these two alloys is achieved by the appropriate heat treatment.

Alloy	Si	Fe	Cu	Mn	Mg	Ni	Zn	Pb + Sn	Ti
A356	6.7				0.30				0.10
	7.3	0.14	0.04	0.09	0.40	0.04	0.09	0.02	0.13
A357	6.7				0.50				0.10
	7.3	0.14	0.04	0.09	0.60	0.04	0.09	0.02	0.15

Table 1.1: Composition of A356 and A357 alloys [9]

Alloy	Casting Method	Young's Modulus MPa	UTS MPa	YS MPa	percent elong.	Hdn Brinell
A356	Sand	74000	270	200	5	90
	Permanent		280	200	16	90
A357	Sand	74000	275	250	1.5	100
	Permanent		330	290	9	110

Table 1.2: Mechanical properties of A356 and A357 alloys (T6) [9]

2. **FACTORS INFLUENCING MECHANICAL PROPERTIES**

Besides heat treatment processing, microstructure determines the strength of a cast Al-Si component. Microstructure hinges on both the composition of the alloy and the casting process.

2.1 **Iron content**

As mentioned earlier, iron bearing intermetallic compounds greatly reduce elongation. Thus, iron is kept at a low level. However, although ingots have a controlled chemistry, incidental introduction of iron in the melt may happen if improperly coated tools are used. Fortunately, most foundries which produce high quality castings possess a spectrometer to control the melt chemistry prior to pouring. Incidental pollution can therefore be readily detected and corrective measures taken.

2.2 **Modification**

The morphology of the eutectic silicon phase can vary from coarse acicular plates to fine fibres upon minute additions of so called modifying elements [10] (Figure 1.5). As silicon is a brittle phase, cracks develop at the interface between the matrix and the silicon particles when the metal is stressed [11]. Alloys in which the silicon is fibrous exhibit a higher elongation than do alloys with plate like silicon particles which tend to act as stress raisers. The mechanical properties of modified and unmodified A356 alloy are listed in Table 1.3 [12]. The potential structure of a treated melt evolves with holding time because of losses of modifying element by oxidation or evaporation - potential structure is meant here as the morphology which the eutectic silicon would assume if the melt were allowed to solidify.

Depending on the modifier used, potential modification of a melt can last from 20 minutes to several hours [13]. Methods such as thermal analysis, or more recently electrical conductivity measurement, have been developed to determine the potential degree of modification of a melt. These methods give a result in less than 10 minutes, and so enable foundrymen to ensure whether proper modification will be obtained or a further treatment is necessary.

Alloy	A356				A357			
	Permanent mould		Sand casting		Permanent mould		Sand casting	
Structure	UTS MPa	Elong %	UTS MPa	Elong %	UTS MPa	Elong %	UTS MPa	Elong %
unmodified	290	12	275	2,5	330	10	290	2
modified	290	17	280	6	330	13	285	2,5

Table 1.3 : Mechanical properties of unmodified and modified A356 and A357 alloys [9]

2.3 Porosity

Porosity in castings (Figure 1.4) arises from two phenomena :

- Shrinkage during solidification which leads to the formation of small pores. These pores form at later stages of solidification when contraction cannot be compensated for by liquid feeding. Shrinkage porosity is eliminated by proper use of risers and chills to create a directional solidification from the casting to the risers which are removed afterwards.

- Dissolved hydrogen in molten aluminum also reduces the soundness of castings. Hydrogen has a significant solubility in liquid aluminum and only a slight solubility in solid aluminum [14]. Therefore, almost all of the hydrogen present in the liquid is unable to dissolve in the solid and accumulates at the solidifying interface where it assists in porosity formation. Hydrogen pickup can be avoided if the melt is handled with care and charge materials are dry and clean. In addition, dissolved hydrogen can be removed before casting by various degassing techniques, most of which involve bubbling an inert gas into the melt.

In addition, several methods are available to control the degree of gassing of a melt before casting. The most widely used is the Staube-Pfeiffer test also known as the reduced pressure test which consists of solidifying a sample under partial vacuum to encourage pore formation. The density of the sample provides a good estimation of the gassing of the melt (degree of gassing is estimated afterwards from the density of the sample).

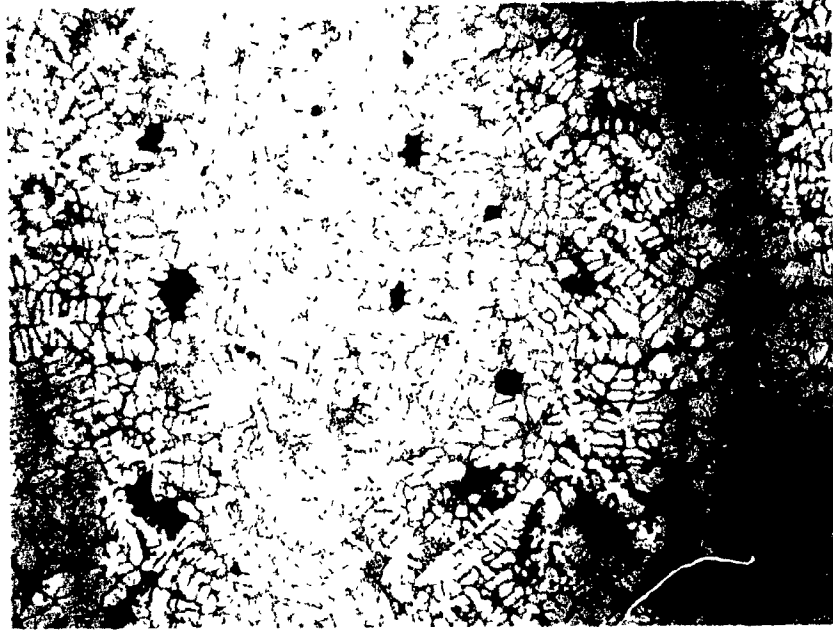


Figure 1.4: Microstructure of as cast A356 alloy exhibiting microporosity as black areas. Mag. X 20

2.4 Dendrite Arm Spacing

A faster solidification rate has an overall beneficial effect on the mechanical properties of a casting. Besides reduction in dendrite arm spacing (Figure 1.6), the increase in tensile strength with increasing solidification rate is also due to less and better distributed porosity, decreasing number and size of intermetallic constituents, and a finer eutectic structure [15]. Solidification rate depends on many factors such as casting conditions and moulding material, and it varies within sections of different thicknesses of a casting.



Figure 1.5 : Microstructures of modified and unmodified A356 alloy. Mag. X 100

Dendrite arm spacing (DAS) is measured only after solidification through measurements on metallographic samples, and thus, unlike iron content, modification and gassing level, it cannot be predicted prior to casting. The correlation between secondary dendrite arm spacing and tensile properties has long been established, and so in principle the DAS could be used to estimate tensile strength; but DAS measurement is a destructive operation, and therefore rarely performed in foundry practice.

Design engineers have traditionally used a safety factor on castings to ensure that adequate strength will be obtained. If a nondestructive technique were devised to determine the DAS at various locations within a casting, then tensile properties could be more accurately predicted.

Moreover, high quality aircraft castings often have highly stressed designated areas where the high mechanical properties required necessitate the use of chills to achieve a rapid solidification rate. However, these chills alter the solidification of the casting and often lead to shrinkage defects. Non destructively measuring DAS may help optimize the chill design to achieve the required mechanical properties while keeping changes in the solidification pattern to a minimum.

3. AIM OF THE PRESENT RESEARCH

The aim of the present research was to determine the feasibility of using electrical conductivity measurements to evaluate variations in secondary dendrite arm spacing within a casting. An earlier study by Argo, Drew and Gruzleski [16] gave evidence that a change in DAS is associated with a detectable change in electrical conductivity in most of the commercial Al-Si alloys except those having a high magnesium content. Since several metallurgical factors affect the overall conductivity of an alloy, the purpose of this research was to isolate and rank the influence of each of these factors, particularly that of DAS.



DAS = 13.5 μm



DAS = 48.5 μm

Figure 1.6 : Microstructures of as cast A356 alloy with different DAS. Mag. X 100

CHAPTER 2

THEORETICAL BACKGROUND AND LITERATURE REVIEW

As the present research deals with secondary dendrite arm spacing and modification in Al-Si alloys, these metallurgical features will be discussed. A brief presentation of the theory of electrical resistivity of metals and alloys will first be given, and then the applications of electrical conductivity in the metallurgy of Al-Si alloys will be reviewed.

1. THEORY OF ELECTRICAL CONDUCTIVITY/RESISTIVITY

1.1 Pure Metals

One of the most well known characteristics of metals is their ability to conduct electricity. This characteristic has been widely investigated by physicists, and several theories have been successively proposed while the knowledge of atom structure and properties was growing.

Earlier theories suggested that electrical properties of a metal were due to the presence of free electrons which detach from the atoms and transfer electric current under an applied electric field [17]. The resistance to electron flow i.e. electrical resistivity was caused by collision with the atoms in the lattice.

Quantum mechanics provided a better understanding of the dual wave-like and particle-like behaviour of electrons. It indicates that only a few electrons which are near the Fermi surface are involved in conduction.

The expression of electrical conductivity as given by quantum mechanics is :

$$\sigma = \frac{Ne^2l}{mV_f}$$

where :

- σ = electrical conductivity
- m = mass of an electron
- e = charge of an electron
- V_f = velocity of the electrons at the Fermi level
- N = number of electron at the Fermi level
- l = mean free path of the electrons

Metals which have partially filled valence bonds and therefore a high density of electrons near the Fermi level exhibit a high electrical conductivity. For a given element, N and V_f are constant so that conductivity is only influenced by changes in the mean free path.

The mean free path of electrons is limited by the process of electron scattering. Electron scattering has two major causes .

- thermal scattering which arises from the interactions between electrons and atomic vibrations (phonons) whose amplitude increases with increasing temperature. Since the higher the vibration amplitude, the more likely an electron collision with an atom is to occur, the mean free path decreases with increasing temperature and so does conductivity. At room temperature, the effect of temperature on the resistivity of metals is approximately linear with a slope equal to $0.00113 \mu\Omega \cdot \text{cm} \cdot \text{K}^{-1}$ for aluminum [17,18],

- impurity scattering which arises from lattice defects such as dislocations, grain boundaries etc. or impurity atoms in solid solution which cause a distortion of the lattice due to their different size and valence. At a given temperature, electrical conductivity decreases as the density of defects causing electron scattering increases [19,20,21].

For very dilute alloys , the effect of impurities on electrical conductivity is expressed as [22,23] :

$$\rho_{\text{imp}} = \frac{mV_f}{Ne^2} \times \frac{X_i}{a}$$

where : X_i = atomic fraction of impurities
 a = interatomic distance
 ρ_{imp} = resistivity due to impurities

These two causes of electron scattering are independent and therefore have additive effects [22,23] on electrical resistivity :

$$\rho_{\text{total}} = \rho_{\text{th}} + \rho_{\text{imp}}$$

where: ρ_{th} = temperature effect
 ρ_{imp} = impurity effect

This relation is known as Mathiessens's rule.

1.2 Alloys

The electrical conductivity of alloys differs from that of pure elements in that the impurity component of resistivity becomes the predominant factor. However the effect of alloying elements not only depends on their concentration but also on the difference of their atomic structure with that of the host metal and on their state in the matrix.

1.21 Solid solutions

In general, the electrical resistivity of a metal is increased by the presence of atoms in solid solution. This increase is given by Nordheims rule [24] :

$$\Delta\rho_0 = A X (1 - X)$$

where : X = atomic fraction of the solute element
 A = a constant which depends on the difference in valence and atomic size between the solute and the solvent elements

If more than one element is dissolved in solid solution their effects are additive [19,22,26], i.e.

$$\Delta\rho_0 = \sum_i A_i X_i (1 - X_i)$$

Table 2.1 [1,18,26,27] lists the available data on the effect of some alloying elements on the resistivity of aluminum.

The resistivity of supersaturated solid solution alloys generally decreases when precipitation of the alloying elements occurs. This results from the fact that solvent atoms in solid solution scatter electrons more effectively than do precipitates [26,28].

Element	r_e/r_{Al} (1)	Solubility (2) (at %)	$\Delta\rho$ (3) ($\mu\Omega$ cm/at. %)
Ag	1.01	24	1.0
Cr	0.984	0.38	8.4
Cu	0.898	2.4	0.83
Fe	0.893	0.025	5.4
Mg	1.12	17	0.46
Mn	0.903	0.90	6.9
Ni	0.870	0.023	1.6
Si	0.978	1.6	0.72
Ti	1.02	0.14	5.5
Zn	0.972	66	0.23

- (1) ratio of atomic radius of element to that of aluminum
- (2) maximum solid solubility of element in aluminum
- (3) resistivity increment per atomic percent of element dissolved in aluminum

Table 2.1: Effect of alloying elements on the resistivity of pure aluminum

1.22 Multiphase alloys

When an alloy consists of more than one phase, the overall electrical conductivity depends not only on the respective resistivities of component phases and their volume fraction, but also on their structural arrangement. The electrical conductivity of a mixture constituted of spherical particles dispersed in a continuous matrix is given by [29] :

$$\sigma_m = \sigma_c \frac{\left(1 + 2 V_d \left(\frac{1 - \frac{\sigma_c}{\sigma_d}}{2 \frac{\sigma_c}{\sigma_d} + 1} \right) \right)}{\left(1 - V_d \left(\frac{1 - \frac{\sigma_c}{\sigma_d}}{2 \frac{\sigma_c}{\sigma_d} + 1} \right) \right)}$$

where : σ_c = conductivity of the continuous phase
 σ_d = conductivity of the dispersed phase
 V_d = volume fraction of the dispersed phase

However, phases in metallic solids often have more complex shapes and thus the resistivity of the mixture follows more complex relationships.

2. MODIFICATION OF EUTECTIC SILICON

In conventional solidification of Al-Si alloys containing more than 1.6% of silicon, a binary eutectic consisting of pure silicon flakes embedded in an aluminum matrix forms at latter stages of solidification [1]. Such a shape is detrimental for the mechanical properties and elongation in particular since the flakes act as stress concentrators when the alloy is strained [30,31]. However, under certain conditions, the microstructure of eutectic silicon can be converted to a fine fibrous morphology [32] less harmful for the elongation. The transformation from a coarse flake to a fine fibrous morphology is termed modification.

The flake-fibre transition can occur either at fast solidification rates or upon addition of specific modifying elements to the molten alloy, such as sodium or strontium.

At fast solidification rates, an Al-Si alloy is undercooled to 10 to 12°C below the equilibrium eutectic temperature before nucleation of silicon particles occurs so that nucleated silicon particles grow very rapidly yielding a fibrous structure [33]. Steen and Hellawell [34] showed that the flake-fibre transition occurs at velocities of 400 $\mu\text{m}\cdot\text{sec}^{-1}$. Such high velocities are however not achievable in common foundry practice.

Additions of sodium or strontium yield the same changes of microstructure as fast cooling but at slower cooling rates. The mechanisms of modification are rather complex and not yet fully understood. Recent theories suggest that modifying elements alter both the nucleation and growth of the eutectic silicon phase.

2.1 Nucleation of Silicon

Nucleation of silicon in Al-Si alloys occurs on particles of aluminum phosphide, AlP, whose crystal structure is very close to that of silicon [35]. In commercial alloys, phosphorous is present as an impurity in amounts of the order of 5 ppm so that a large quantity of AlP nuclei forms in the melt. Consequently, eutectic silicon nucleates at low undercoolings ($<2^{\circ}\text{C}$) and grows in a coarse flake morphology [35]. Modifying elements neutralize AlP nuclei causing silicon nucleation at higher undercoolings, and a more rapid growth, since the driving force for growth, which is proportional to the undercooling, is greater. However, the reduction of the number of nuclei alone does not account for the observed fibrous morphology. Indeed, fewer nuclei result in a finer acicular structure but do not promote any change in morphology. Therefore, in order to achieve a fibrous structure, the modifying elements must also alter the growth mechanism of the eutectic silicon particles.

2.2 Growth of eutectic silicon particles

In unmodified alloys, the eutectic silicon phase grows as thin flat plates in a faceted manner ahead of the aluminum rich phase [32]. This type of growth occurs by the twin plane re-entrant edge mechanism (TPRE) [36] in the close packed $\{111\}$ plane which is also the twinning plane. The TPRE mechanism is illustrated schematically in Figure 2.1

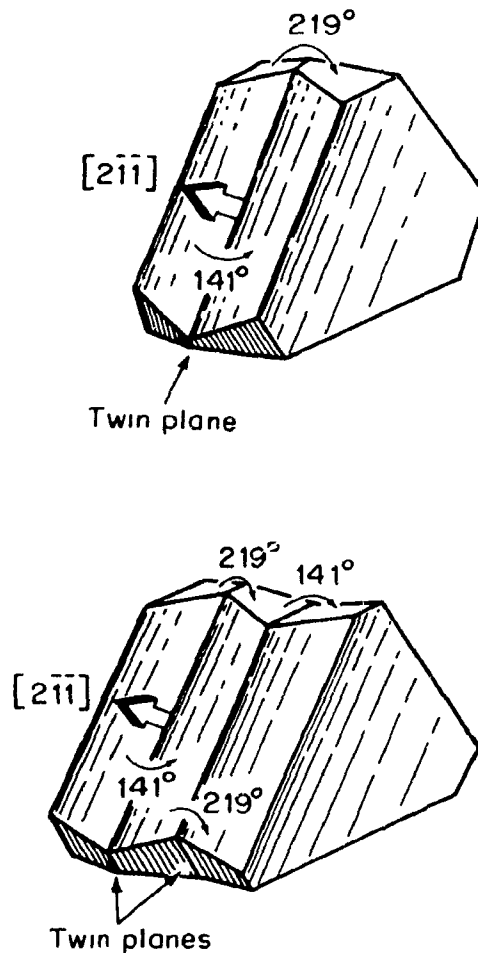
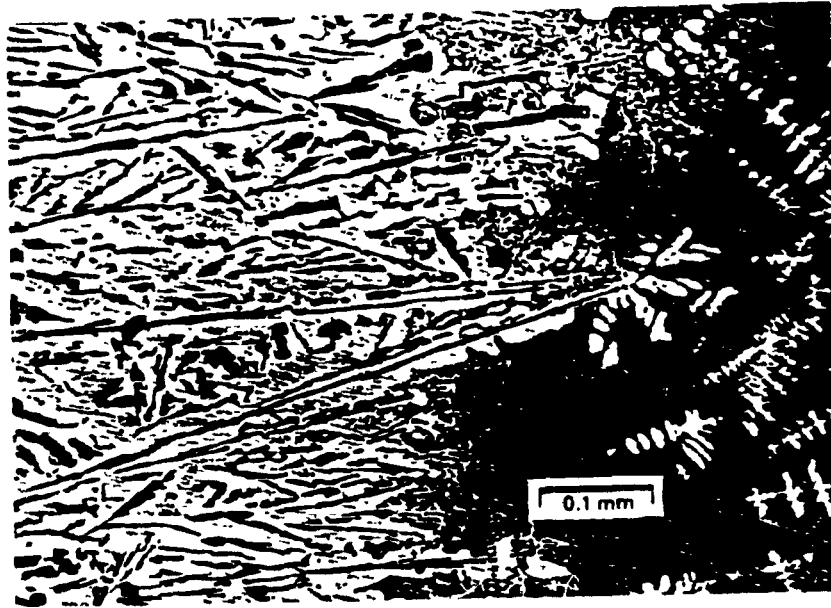


Figure 2.1: The TPRE growth mechanism [37]

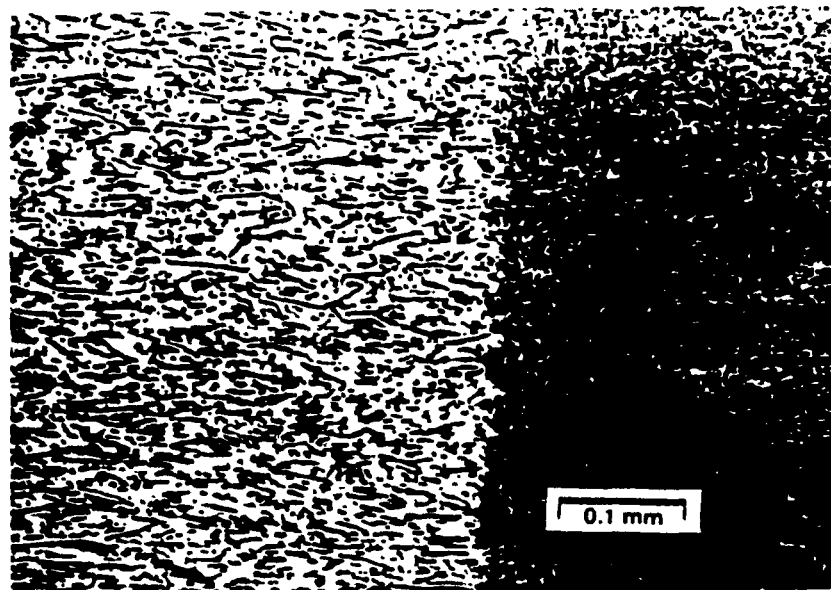
[37,38]. Silicon growth is anisotropic, the slowest growth direction being normal to the {111} plane. When a twin plane emerges at the growing interface, growth takes place rapidly in the $\langle 211 \rangle$ directions until these preferential growth sites disappear. However, if two twin planes are present at the interface, the favoured growth sites at the $\langle 211 \rangle$ directions do not disappear and growth continues indefinitely yielding flat silicon flakes.

When a modifier is added to the melt, growth by the TPPE mechanism in $\langle 211 \rangle$ directions is poisoned by selective adsorption of modifier atoms onto the preferential growth sites [39] so that silicon growth becomes more isotropic and eutectic silicon particles assume a branched fibrous morphology.

Another consequence of the adsorption of atoms of modifier on specific crystallographic planes is the removal of the silicon lead at the growth interface which becomes planar resulting in coupled growth (Figure 2.2) [32,39].



a) unmodified



b) modified

Figure 2.2 : Solid-liquid interfaces in Al-Si eutectic alloys [32]

3. DENDRITE ARM SPACING

Dendrite arm spacing is a structural feature defined as the distance between two adjacent secondary dendrite arms (Figure 2.3). It has had an increasing interest for the metallurgist in recent years since it provides a quantitative indication of structural refinement which has a direct bearing on the mechanical behaviour of a cast material.

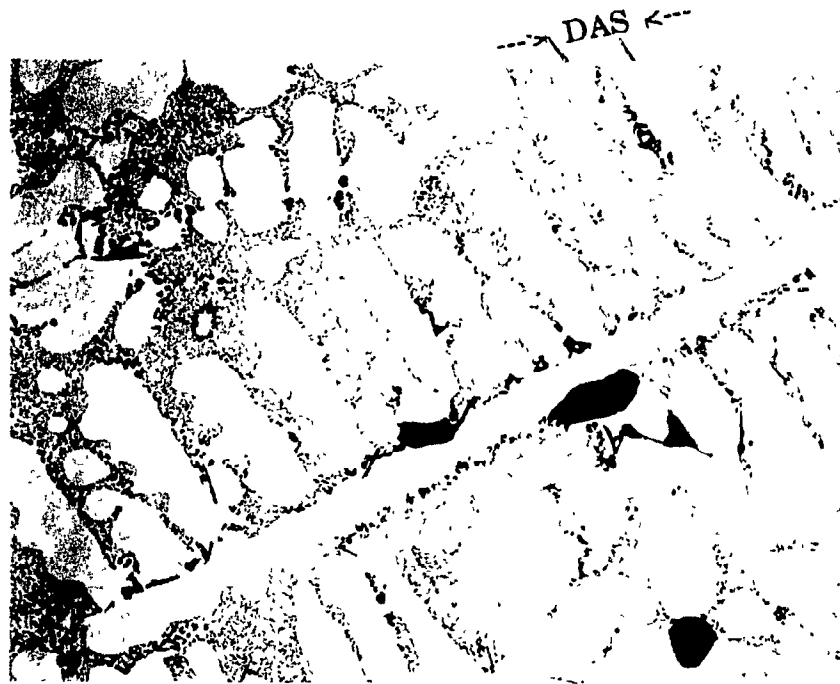


Figure 2.3 : Definition of the Dendrite Arm Spacing

3.1 Dendritic solidification

Aluminum, as other metals, solidifies in a dendritic manner when alloyed. Dendrite formation arises from constitutional undercooling in the liquid ahead of the solid-liquid interface owing to solute rejection at the solidification front [37,38,40]. In alloy solidification, the solid which forms has a different composition from that of the parent liquid so that a solute rich boundary layer progressively builds up in front of the solidifying interface as diffusion in the solid is too slow for homogenisation to occur.

Accordingly, the equilibrium liquidus temperature (T_l) increases from the interface to the bulk liquid (Fig. 2.4). Therefore, if the temperature gradient ahead of the growth interface $\frac{dT_l}{dz}$ is smaller than a critical value, the solute rich boundary layer is undercooled over a certain distance so that the interface becomes unstable. The instability gives rise to the formation of protuberances or cells parallel to the heat flow which turn into dendrites growing in the preferred crystallographic growth direction as growth rate increases and crystallographic effects become more important. As growth rate further increases, secondary arms begin to form. Researchers have shown that secondary dendrite arm spacing is controlled by the cooling rate during solidification and the composition of the alloy [37,41]. It follows approximately the relationship :

$$d = at_f^{1/3} = \frac{b}{(\text{cooling rate})^{1/3}}$$

Where a and b are constants

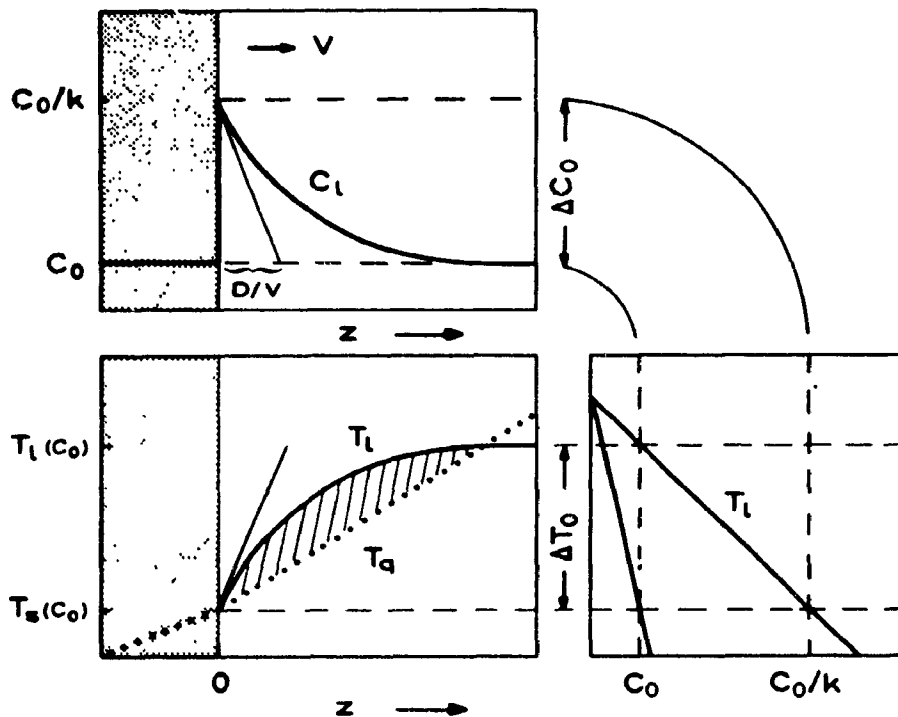


Figure 2.4: Constitutional undercooling [38]

The initial secondary dendrite arm morphology evolves as solidification progresses [37] so that the spacing measured in fully solidified casting is coarser than that initially formed.

Coarsening arises from the remelting of some of the arms owing to surface energy differences between adjacent arms. Indeed, back from the dendrite tip, constitutional undercooling which is the driving force for arm formation, is greatly reduced so that the effect of curvature on melting point becomes important. Three mechanisms [62] were established after studies on isothermal coarsening to account for the remelting of the arms. These mechanisms are sketched in Figure 2.5. The equilibrium temperature of a liquid-solid interface is depressed as the radius of curvature of the interface becomes smaller.

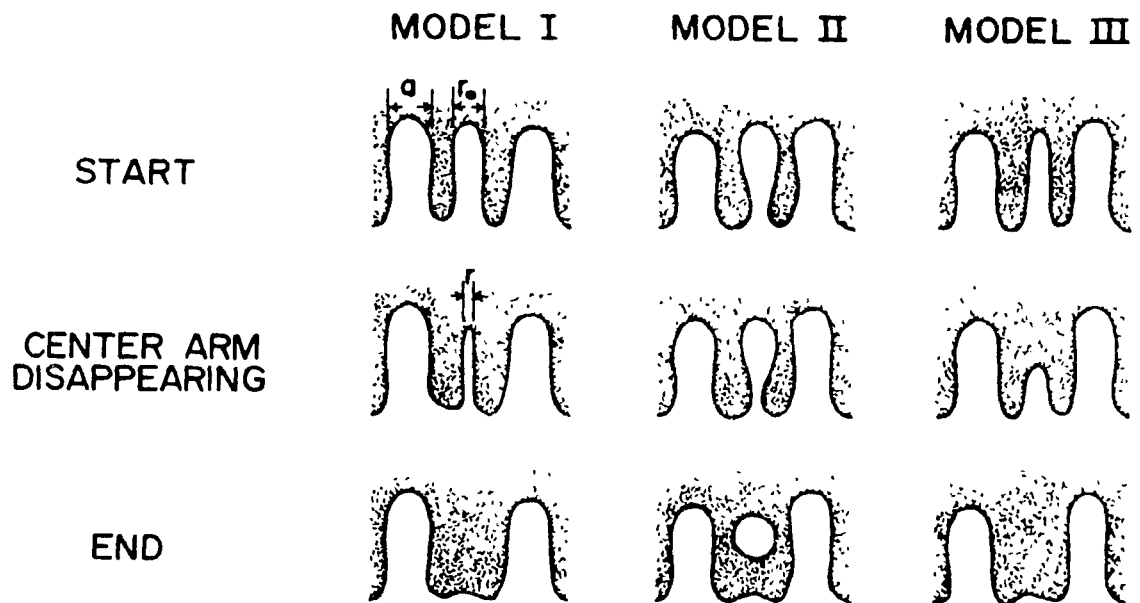


Figure 2.5 : Mechanisms of dendrite arm coarsening [37]

Hence, two arms of different radii of curvature at a fixed temperature will be in equilibrium with liquid of different compositions. Therefore, a diffusion couple is created in the liquid between the two dendrite arms resulting in the remelting of the arm of smaller radius of curvature. Consequently, the amount of time the alloy remains in the solidification range i.e. the interval of temperature in which dendrites grow, has a direct bearing on the final coarseness of the dendritic structure. This interval depends on the cooling rate throughout solidification as well as the solidification range which varies with the composition of the alloy.

3.2 Importance of dendrite arm spacing

Secondary dendrite arm spacing as an indication of microstructural refinement is of particular importance for predicting the mechanical properties of a casting at a critical location. Spear and Gardner [41] have shown that, for aluminum alloys, elongation and tensile strength increase with decreasing dendrite cell size (Figure 2.6) - dendrite cell size is the width of an individual dendrite cell, and, like dendrite arm spacing, may be used to describe dendrite refinement. Yield strength is essentially unaffected (Figure 2.6). These results, confirmed by several other researchers [15,42,43], are attributed to the reduction in size and the more even distribution of porosity and intermetallic compounds with decreasing dendrite cell size.

Frederick and Bailey [44] later concluded from studies carried out on cast 356 aluminum alloy that variations in strength are a consequence of variation in ductility which is inversely proportional to the dendrite cell size.

They proposed a mechanism to account for the relationship between ductility and inverse cell size based on differential strain across dendrite cell boundaries and fracture strain of eutectic silicon particles. Bailey [45] and recently Scholin [46] showed that fatigue properties are inversely proportional to the square root of dendrite arm spacing.

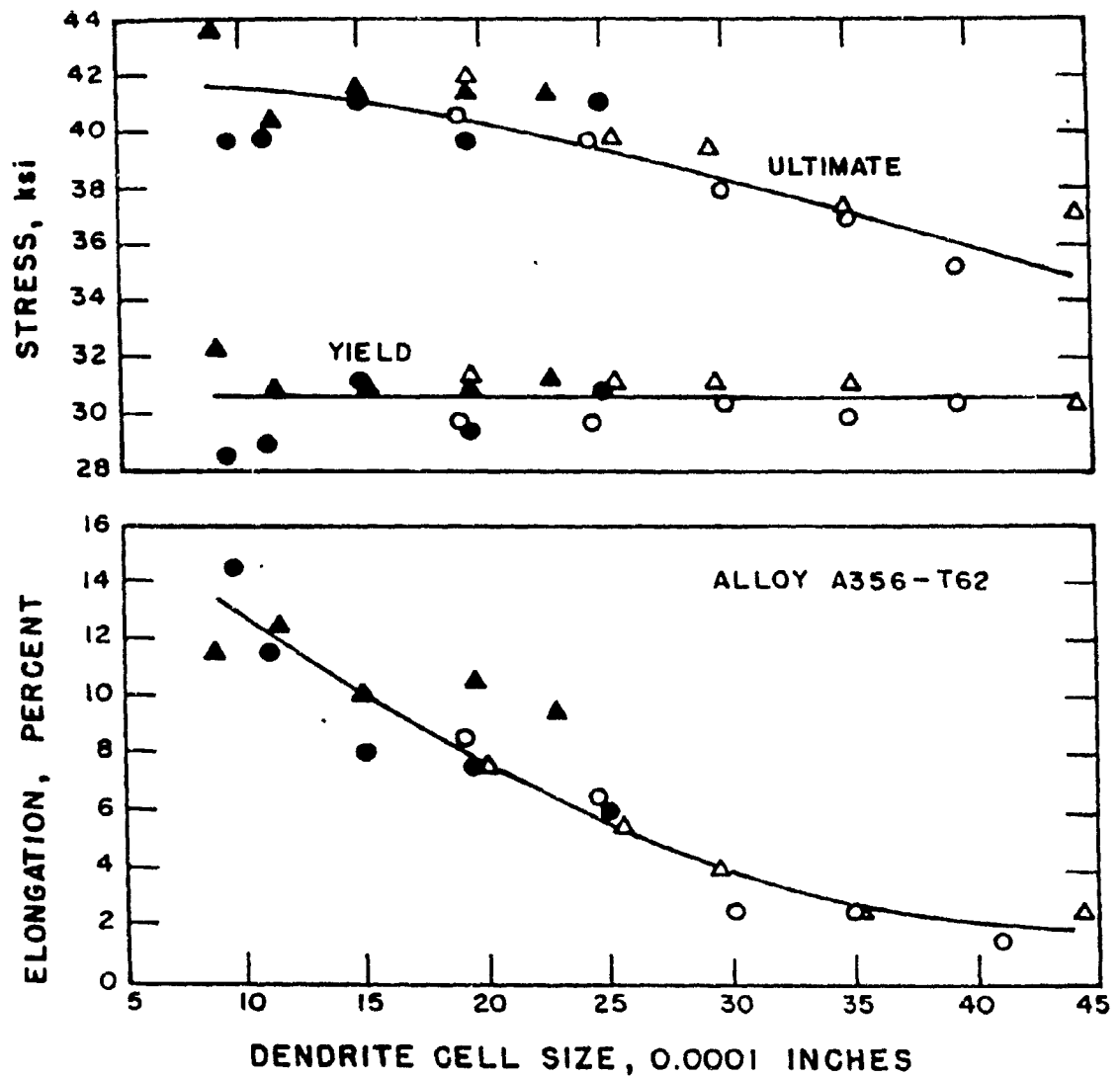


Figure 2.6 : Tensile properties variation with dendrite cell size of 356.T6 alloy [41]

Dendrite arm spacing also directly impinges on the effectiveness of a solution treatment [37], the reason for this being that elements from non equilibrium intermetallic compounds have to diffuse over a distance equal to the thickness of a dendrite arm during homogenisation of the aluminum matrix by solution treatment.

4. APPLICATION OF ELECTRICAL CONDUCTIVITY IN METALLURGY OF Al-Si CASTING ALLOYS

4.1 Assessment of the degree of modification

Several studies have been conducted on the applicability of electrical conductivity measurements to non destructively predict modification in a casting. As early as 1959, W. Patterson and D. Amman [47] reported an increase in electrical conductivity as the eutectic silicon morphology alters from granular to fibrous. Thirmavukkarasu and Panchanatan⁴⁸ made the first attempt to use electrical conductivity to assess modification in Al-Si alloys in 1978. In 1983, Jacob and Remy [49] used an electrical conductivity measurement technique based on eddy current while Oger, Closset and Gruzleski [50] applied a DC resistivity technique to study the morphology changes occurring during modification. These latter authors next used an AC differential resistivity measurement technique [51] based on the difference in voltage between a standard unmodified sample and a Sr modified one.

These studies showed that the electrical conductivity of modified alloy is higher than that of unmodified alloy, the difference between the two being 5% or more. The difference in conductivity increases as the silicon becomes finer i.e. as the degree of modification is enhanced.

Jacob et al. [49] and Mulazimoglu et al. [52] demonstrated that resistivity of unmodified alloys decreases linearly with increasing silicon content, whereas for modified alloys the rate of decrease diminishes as the silicon content increases to approach zero near the eutectic composition (Fig. 2.7). Therefore, the difference in conductivity between unmodified and modified alloys also increases with increasing silicon content.

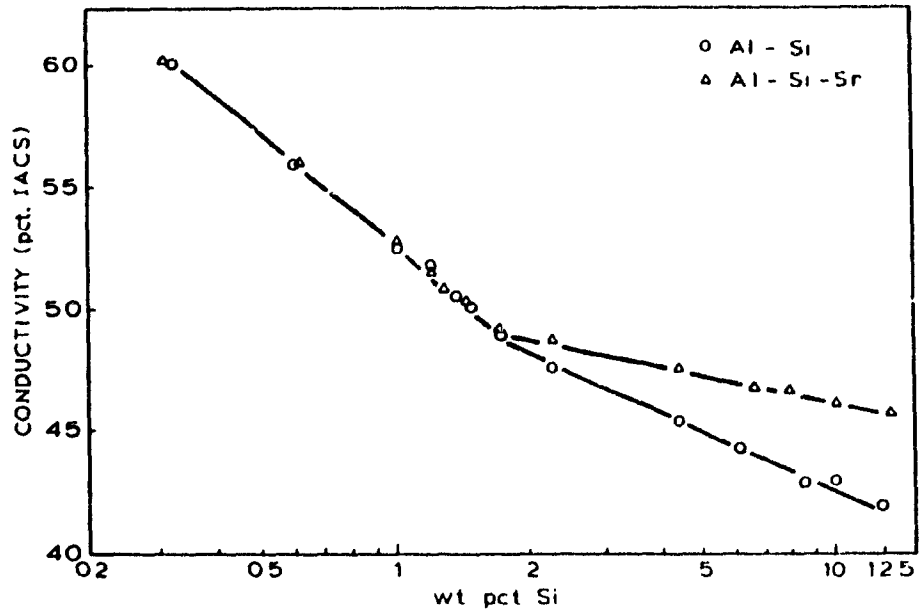
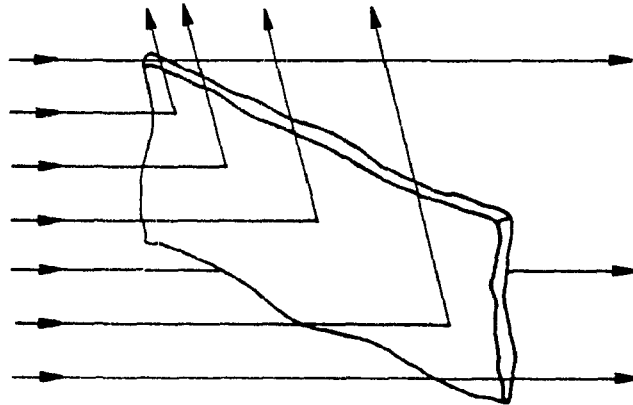


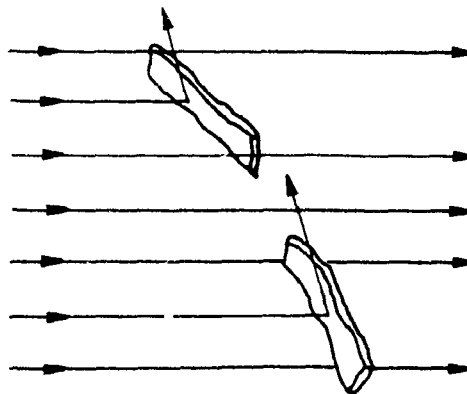
Figure 2.7: Conductivity variation with silicon content for modified and unmodified A356 alloy [53]

Recently, Mulazimoglu [53] explained the observed increase in conductivity with modification by considering the effect of the structural change on the electron scattering from the eutectic silicon-aluminum matrix interface.

Silicon fibres allow easier electron flow than do plates because the projected interfacial area between silicon particles and the aluminum matrix is smaller for fibres than for plates. This is illustrated in Figure 2.8.



(a) Unmodified



(b) Modified

Figure 2.8 : Mechanism of electron scattering at Al-Si interface [53]

Several authors have reported that modification cannot be detected by electrical conductivity measurements in high magnesium containing alloys such as A355 and A357 (0.6% Mg).

Closset et al. [51] explained this by the refining effect of magnesium on the silicon morphology; electrical conductivity changes with modification are consequently too small to be detected.

Microporosity also reduces electrical conductivity by impeding electron flow [16,50]. However, most acceptable castings have densities which vary within a very small range, and conductivity is therefore nearly unchanged by porosity.

4.2 Heat treatment

Electrical conductivity has found commercial application for the continuous control of heat treatment of aluminum alloys owing to the large changes in conductivity accompanying the decomposition of supersaturated solid solutions. Indeed, as mentioned in chapter 1 section 1.21, the presence of alloying elements in solid solution decreases electrical conductivity, and precipitation would therefore be expected to increase conductivity. This is true if precipitates are not coherent with the matrix. However, if precipitates have coherent interfaces with the matrix as is the case for hardening phases which precipitate through different stages of the growth of clusters having an epitaxial relationship with the matrix, conductivity decreases initially to further increase as the particles lose their coherency while reaching their equilibrium composition. The increase in conductivity is attributed to the formation of coherent Guinier-Preston zones (G.P. zones) [28] which add a large strain to the lattice as they grow. The number of G.P. zones has a direct bearing on hardness and yield and tensile strength of age hardenable alloys with the maximum of mechanical properties reached when the number of G.P. zones is greatest (i.e. the conductivity is a minimum).

Hence, electrical conductivity can be readily used to follow clustering kinetics during aging treatments so as to accurately determine optimum aging time and temperature, and to monitor commercial heat treatments of precipitation hardening alloys.

An increase in resistivity at early stages of aging at low temperatures has been observed in the Al-Ag, Al-Cu, Al-Mg, Al-Zn and Al-Mg-Si alloy systems. However, Rosenbaum and Turnbull [54] did not detect any changes in resistivity in Al-Si alloys at low temperature but observed a continuous drop during aging at higher temperature (150-360°C). They suggested that there is no G.P. zone formation in Al-Si alloys.

4.3 Application to Al-Si-Mg alloys

Electrical conductivity changes are also observed in Al-Si-Mg alloys during solution treatment carried out near the eutectic temperature, usually at 540°C. Investigations showed that electrical resistivity increases on solution treatment, and that modified alloys exhibit higher changes than unmodified alloys. Closset et al. [55,56] suggested that the observed increase in resistivity is due to the combined effects of Mg_2Si phase dissolution in the aluminum matrix and spheroidisation of the eutectic silicon particles. The dissolution process increases electrical resistivity whereas spheroidisation has the opposite effect. Unmodified alloys are more affected by spheroidisation since the as cast structure is coarser. Thus, electrical conductivity changes with the spheroidisation of the acicular silicon plates are higher than for silicon fibres.

Mulazimoglu recently investigated the electrical conductivity changes in Al-Si-Mg alloys during solution treatment at 540°C as a function of time [53,57]. He reported three definite stages in the solution treatment as shown in Figure 2.9.

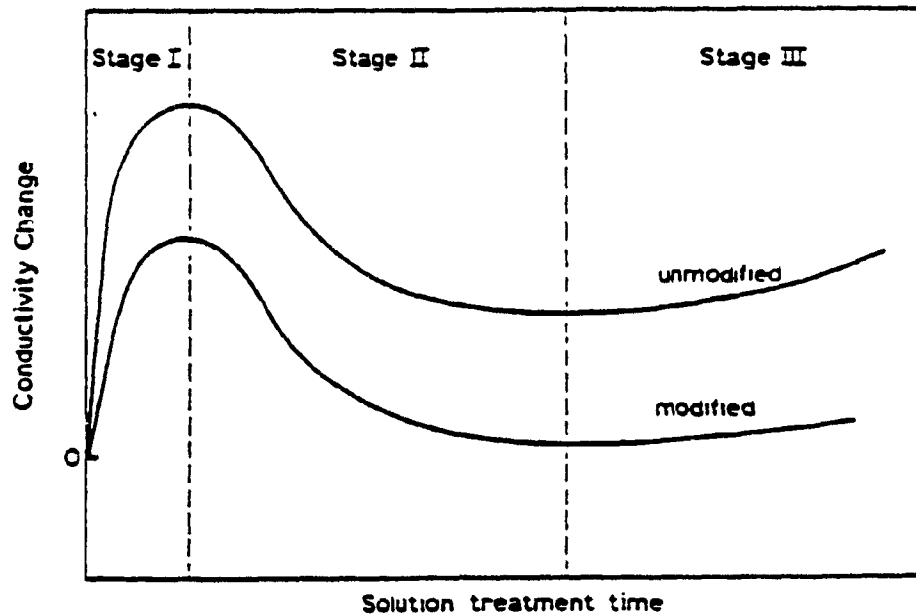


Figure 2.9 : Stages of conductivity changes during solution treatment [53]

The first stage during which conductivity increases is characterized by the precipitation of Mg_2Si and silicon out of solid solution. The second stage corresponds to the dissolution of precipitates together with the spheroidisation of the silicon. Finally, in the third stage, coarsening of the spheroidized silicon occurs without significantly changing the conductivity.

4.4 Determination of dendrite arm spacing

The feasibility of determining secondary dendrite arm spacing by electrical conductivity measurements has been investigated by Argo, Drew and Gruzleski [16] on several Al-Si casting alloys. These authors have developed a DAS measurement technique based on comparative conductivity measurements on a test casting and the casting to be inspected where both are cast from the same melt.

They demonstrated that electrical conductivity decreases linearly with increasing DAS, and that the decline is more pronounced for modified alloys as seen in Figure 2.10. This technique gives a reliable prediction of DAS in modified 319, 355, 356, 357 and 380 alloys but lacks accuracy in unmodified alloys owing to the lower slope of the calibration curve.

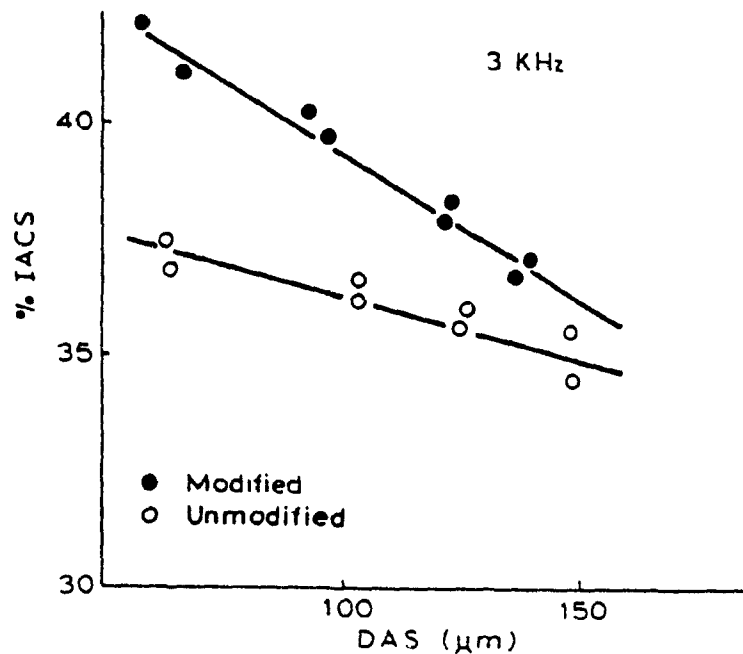


Figure 2-10: Variation of conductivity with DAS on modified and unmodified A356 alloy [16]

CHAPTER 3

EXPERIMENTAL PROCEDURE

The aim of the research was to isolate and quantify the influences of the DAS and modification on the electrical conductivity of common Al-Si foundry alloys by establishing a mathematical model of the type $\sigma = f(\text{DAS}, \text{Modification})$ that could later be used at the foundry level to predict the DAS of castings.

Because of the complexity of the mechanisms involved, it was decided to develop an empirical polynomial model that would best fit the experimental results. Previous studies of the influence of metallurgical features on electrical conductivity reported in Chapter 2 showed that the relationship to expect would be :

$$\sigma = A_0 + A_1 \times \text{DAS} + A_2 \times \text{structure} + A_3 \times \text{DAS} \times \text{structure} + A_4 \times \text{structure}^2 + A_5 \times \text{DAS}^2$$

Since this relation involves a second order term in structure, at least three levels of modification were required for each alloy. In addition, at least two replications of one experiment (same melt chemistry) were also required to have an indication of the variability of the conductivity values.

1. DESIGN OF THE CASTING

To achieve various cooling rates (and hence various DAS values), a step casting was designed as shown in Figure 3.1. The dimensions of the riser and the filling system were calculated according to the gating and risering rules established for aircraft quality castings [59].

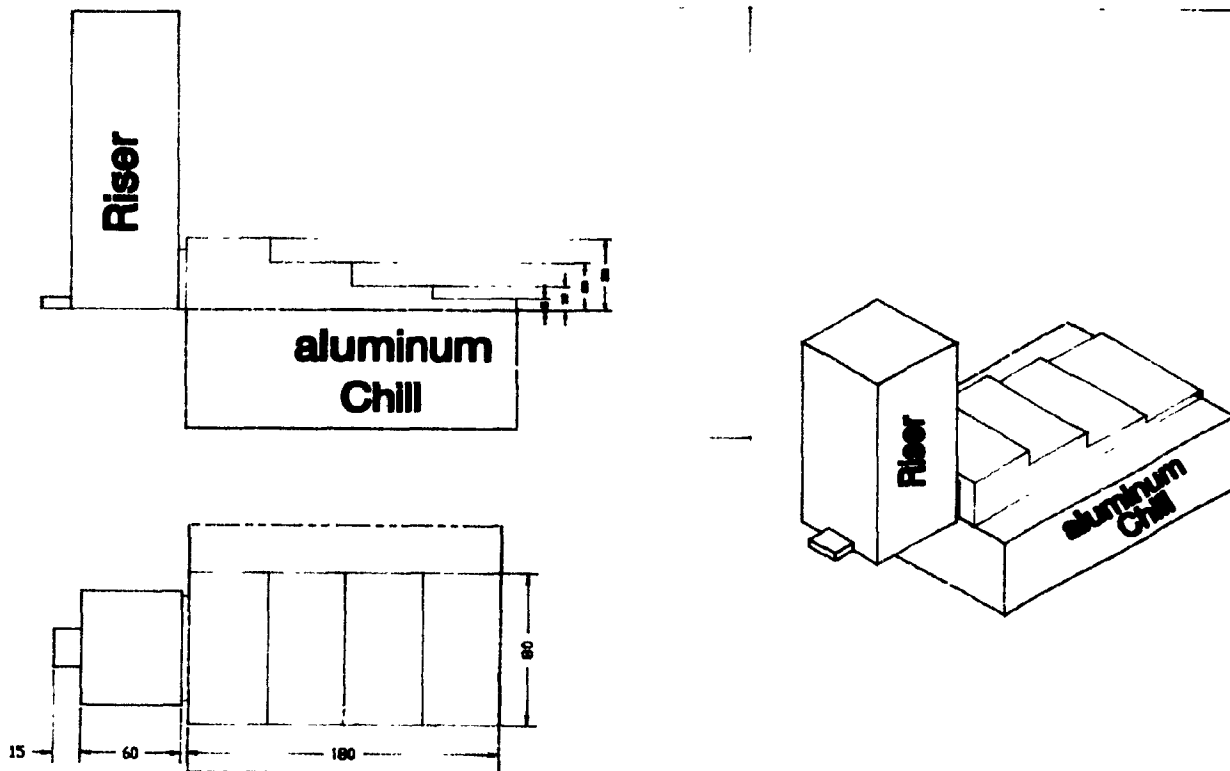
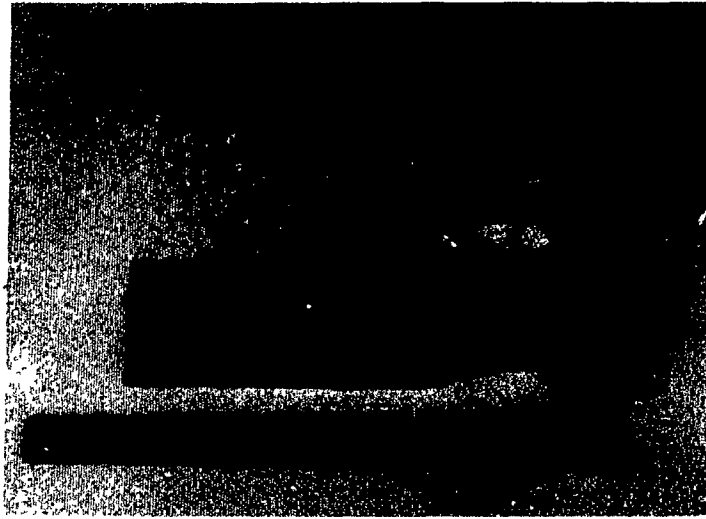


Figure 3.1 : Step casting (dimensions in mm)

Such a design guarantees a quiescent mould filling and feeding of the last solidifying zone. An entirely sound casting free of any oxide is thereby ensured. In order to enlarge the range of cooling rates to those usually achieved in permanent mould casting, an aluminum chill was placed underneath the casting in one of the moulds as shown in Figure 3.2. The chill surface was coated with a thin layer of mould coating so as to avoid welding of the casting by chill surface melting during pouring of the molten metal into the mould.

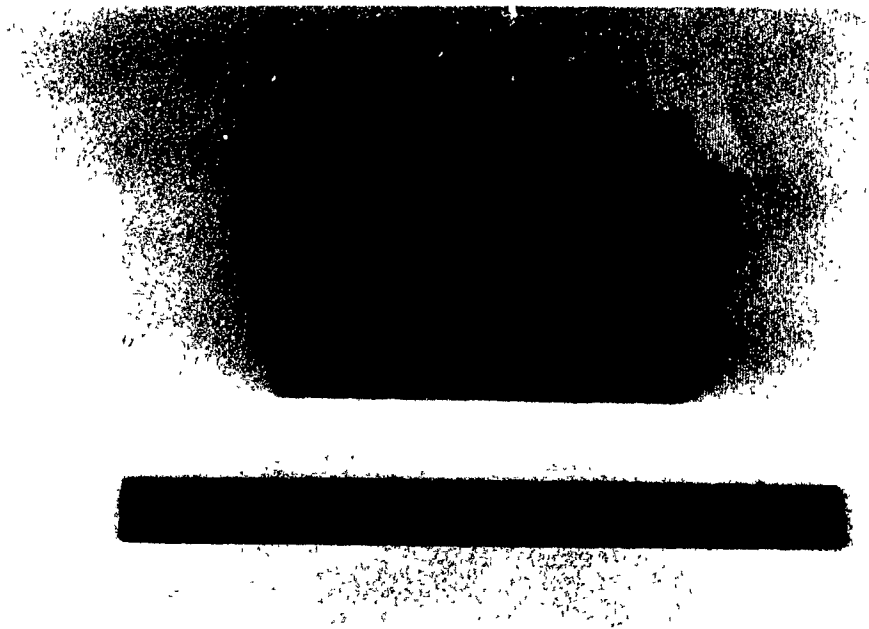


Figure 3.2 : Aluminum chill

2. MATERIALS

2.1 Moulding

The castings were cast in sand moulds manufactured from Petrobond sand mixture. The silica sand used in that mixture had a grain size of 140 according to the rating scale defined by the American Foundrymen's Society. This type of moulding process does not require any baking or curing of the sand, the cohesion being ensured by the very fine red Petrobond sand and the added oil.

2.2 Alloys

In order to study the influence of magnesium on the conductivity behaviour, two kinds of alloys were used: magnesium free alloys which were synthesized from pure materials, and commercial alloys containing different levels of magnesium which were obtained from primary ingots.

The chemical compositions of the materials used in the preparation of the alloys supplied by the producers are listed in Table 3.1.

- **Synthetic alloys**

- Commercial purity aluminum was produced by Alcan in the form of 23 kg ingots. The purity was 99.7%.
- Silicon was supplied by Johnson Matthey in the form of lumps. The purity was 99.9999% which corresponds to the semiconductor grade.

- Titanium was added in the form of rods of Al-Ti6% Tital® master alloy produced by KB Alloys.
- A356 alloy
The primary ingots of A356 were produced by Alcoa. Each ingot weighed 13.5 kg.
- A357 alloy
The primary ingots of A357 were produced by Belmont Metals Inc., New York.
- Strontium was used as a modifier. It was added in the form of Al-Sr10% master alloy produced by KB Alloys.

Elements	Commercial purity aluminum wt. pct.	A357 wt. pct.	A356 wt. pct.	Tital wt. pct.
Si	0.041	7.02	7.10	0.06
Cu	0.002	0.035	<0.001	-
Fe	0.09	0.066	0.082	0.14
Mg	<0.001	0.510	0.34	-
Mn	0.001	<0.02	<0.02	-
Zn	-	0.03	0.01	-
Ni	-	-	-	-
Cr	-	<0.02	<0.02	-
Ti	0.003	0.01	0.08	6.4
Sr	<0.0001	-	-	-
P	0.0001 0.0002	-	-	-
V	-	-	-	0.034
Al	Balance	Balance	Balance	Balance

Table 3.1 : Chemical compositions of the primary ingots and master alloys used

3. **MELT PROCESSING**

1.3 **Melting and Alloying**

Melting was performed in a 10 kg silicon carbide crucible fired in a gas furnace. Each melt consisted of approximately 7 kg of alloy.

After melting, the melt was brought up to 750°C and maintained within $\pm 5^\circ\text{C}$ of this value. If melt additions were to be made, the elements were plunged into the melt and held at the bottom of the melt with a graphite plunger. After a few seconds, the melt was stirred with the plunger, the elements being still kept at the bottom of the crucible.

In the case of synthetic alloys, silicon was added first into the molten aluminum followed by titanium and finally strontium, if the melt was to be modified. The temperature of the melt was brought back to 750°C between each addition. Finally, a 20 minutes dissolution period was allowed for complete homogenisation before degassing. The levels of strontium introduced were respectively 120 ppm for undermodified melts and 300 ppm for modified melts. These levels were calculated by taking into account the loss occurring during degassing.

3.2 Degassing

Degassing was performed in order to remove dissolved hydrogen from the melt which causes porosity formation during solidification owing to the large difference in solubility of hydrogen in liquid and solid aluminum.

Each melt was degassed by bubbling argon for 25 minutes at a rate of 2.5 l/min through a graphite tube pierced with tiny holes (Fig.3.3).



Figure 3.3 : Degassing technique

3.3 Melt quality control

The melt temperature was controlled using a chromel-alumel K type thermocouple.

Immediately after degassing, a sample was cast into a copper mould for spectrochemical analysis. The efficiency of the degassing process was determined by pouring liquid metal into a steel cup and allowing it to solidify in a vacuum chamber where the pressure was fixed to 80 mbar. The reduction of the pressure encourages hydrogen gas bubble formation [8,58]. After completion of solidification, the density of the sample was measured and compared to the theoretical density of the alloy. The difference between the two densities is indicative of the level of gassing of the melt.

3.4 Casting

The molten alloy was cast into two sand molds, the one containing the aluminum chill being filled first. Immediately after pouring, the risers were covered with insulating glass fibre (Figure 3.4) so as to limit heat losses and maintain the riser in the liquid state longer. By so doing, the riser yields were maximized and the casting solidified free of shrinkage microporosity.

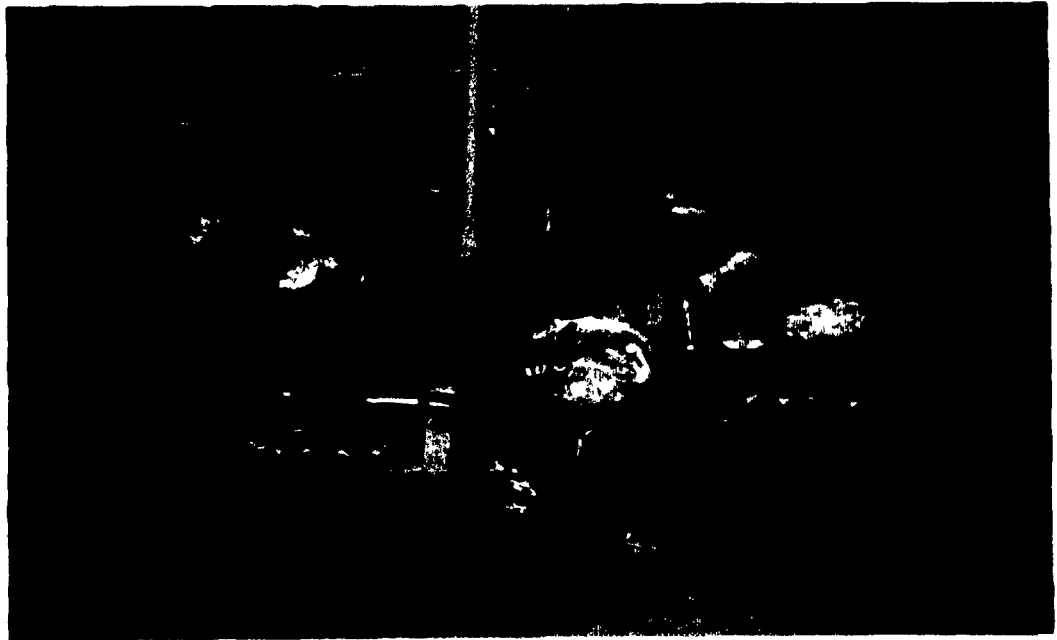


Figure 3.4: Sand moulds after casting

Modified melts were cast exactly one hour after strontium introduction in order to obtain a full efficiency of the strontium as a modifier. The interval of one hour corresponds to the length of time duration of the so called incubation period [58].

The moulds were allowed to cool overnight after which they were emptied and the castings cleaned of attached sand.

3.5 Heat treatment

Two different heat treatments were carried out on some of the castings produced in order to study the evolution of electrical conductivity throughout these treatments.

- 1: a precipitation treatment of 4 hours at 200°C was carried out so as to precipitate elements out of solid solution. The purpose of this treatment was to bring alloys close to equilibrium by enabling elements to diffuse out of any supersaturated solid solutions which formed because of a rapid cooling rate in the solid state after solidification.
- 2: a complete industrial heat treatment consisting of a solution treatment followed by an artificial aging designated as T6 by the Aluminum Association. The procedure adopted in the present study was the following.
 - a solution treatment of 10 hours at 540°C during which intermetallic compounds redissolve into the Al matrix as a result of the increase of solubility with temperature, and further diffuse to yield a homogeneous aluminum matrix. Spheroidisation of the eutectic silicon phase by coalescence also occurs during this treatment.
 - a rapid quenching in room temperature water followed by a pre-aging (natural aging) for 36 hours.
 - an artificial aging performed at 160°C for 6 hours.

This sequence of treatments was done in a programmable electric resistance furnace. The temperature inside the furnace could be controlled with a $\pm 0.5\%$ accuracy. The castings were placed in the central portion of the furnace and the temperature variation was in the range of $\pm 2^\circ\text{C}$.

Electrical conductivity measurements were taken immediately after quenching in water (T4 condition) and after artificial aging when the sample had cooled down to room temperature (T6 condition).

4. SAMPLE CHARACTERISATION

4.1 Electrical conductivity measurements

Electrical conductivity measurements were carried out using a portable eddy current tester, model M1900-10 manufactured by K.J. Law Engineers Inc.. This eddy current tester (Figure 3.5) is a battery operated, rechargeable, hand held instrument capable of operating at 10 different frequencies from 10 Hz to 300 kHz and uses interchangeable probes. It gives a digital readout which, with calibration, can be converted to electrical conductivity.

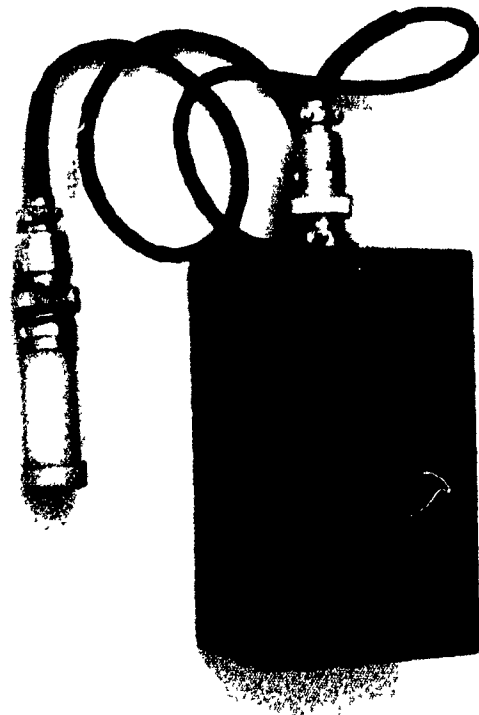


Figure 3.5 : K.J. Law eddy current tester

Eddy current testing consists of inducing an electric current in a conductive material by means of an alternating magnetic field, and observing the resulting interaction between the applied and the induced currents. The alternating magnetic field is generated by passing an alternating electric current through a coil located at the end of the probe.

Coupling the initial magnetic field with a sample is readily achieved by placing the flat ended probe against a flat surface of the test piece without using any coupling agent. Figure 3.6 illustrates the eddy current technique.

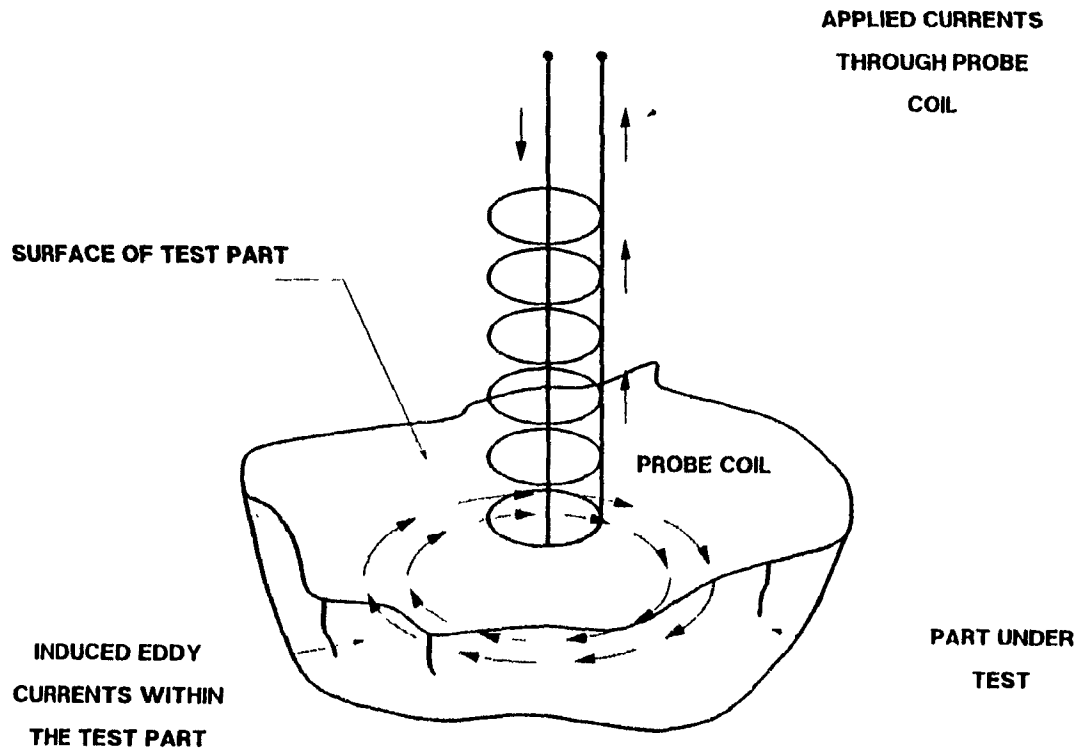


Figure 3.6 : Principle of eddy current technique

The nature of eddy currents depends both on the physical properties of the material and the shape of the sample. The parameters of influence are :

- electrical conductivity
- magnetic permeability
- geometry of the sample
- surface condition of the sample

Al-Si alloys are considered non magnetic, and therefore have a magnetic permeability equal to 1.

The effects of surface condition and geometry of the sample on the eddy current readouts displayed by the K.J. Law M1900 were investigated in a previous study [16]. It has been shown that for 1kHz and 3kHz frequencies, conductivity values measured on an as cast surface and after machining are very close (Figure 3.7).

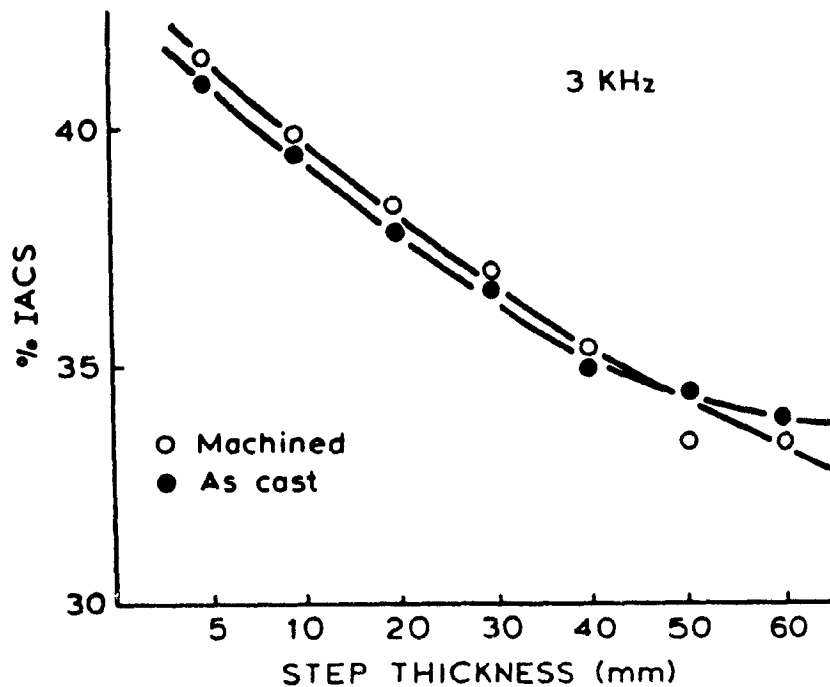


Figure 3.7 : Conductivity readings on as cast and machined surfaces

[16]

Furthermore, the accuracy of the readings decreases rapidly as the depth of penetration of the eddy currents gets closer to the actual thickness of the sample. The depth of penetration is given by the relationship :

$$d \text{ (mm)} = \frac{660}{\sqrt{\sigma \times \mu \times f}}$$

where: d : is the penetration depth in millimeters
 σ : is the electrical conductivity of the material as a percentage of the International Annealed Copper Standard (% IACS)
 μ : is the magnetic permeability
 f : the frequency (Hz) of the alternating current in the coil

As can be seen from the equation, the depth of penetration increases as frequency decreases for a given conductivity.

Figure 3.8 shows the effect of sample thickness on the conductivity of A356 aluminum alloy. Clearly, the lower the test frequency, the greater the penetration depth and therefore the thicker the sample needed for reproducible results. Based on these results a frequency of 3 kHz was chosen for conductivity measurements in the present study. The step casting used had a 5 millimetre thick step, an order of thickness common in real castings, whose conductivity could only be accurately measured with a frequency of 3 kHz. At this frequency, both surface condition and geometry of the sample have little effect on the eddy current readout. Therefore, since magnetic permeability is constant for aluminum as mentioned earlier, the eddy current readout depends only on the electrical conductivity of the sample at 3 kHz. Hence, this value of frequency appears to be the most appropriate for conductivity measurements as far as accuracy is concerned.

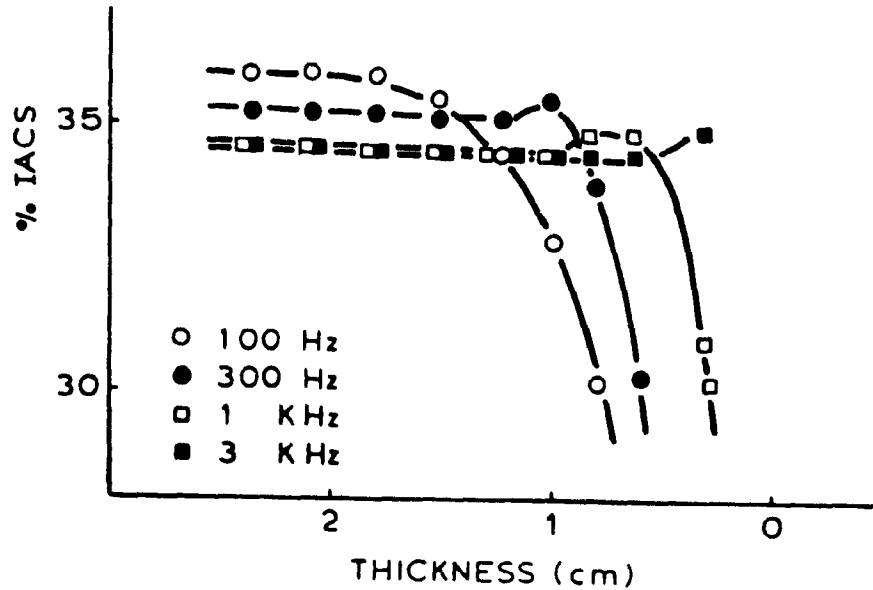


Figure 3.8 : Variation of conductivity with sample thickness [16]

Electrical conductivity was measured on the top of the castings, five readings being taken on each step and the average calculated. In the perspective of an industrial application of the method for the non destructive testing of Al-Si castings, the surface of the samples was left as cast. However, the error in conductivity introduced by measuring on the as cast surface was a minimum because of the frequency used.

As temperature has a significant effect on electrical conductivity, the samples were kept at a constant temperature when measurements were taken.

4.2 Metallography

Metallography was used both to assess modification and to determine the dendrite arm spacing. Metallographic samples were cut from the castings as shown in Figure 3.9.

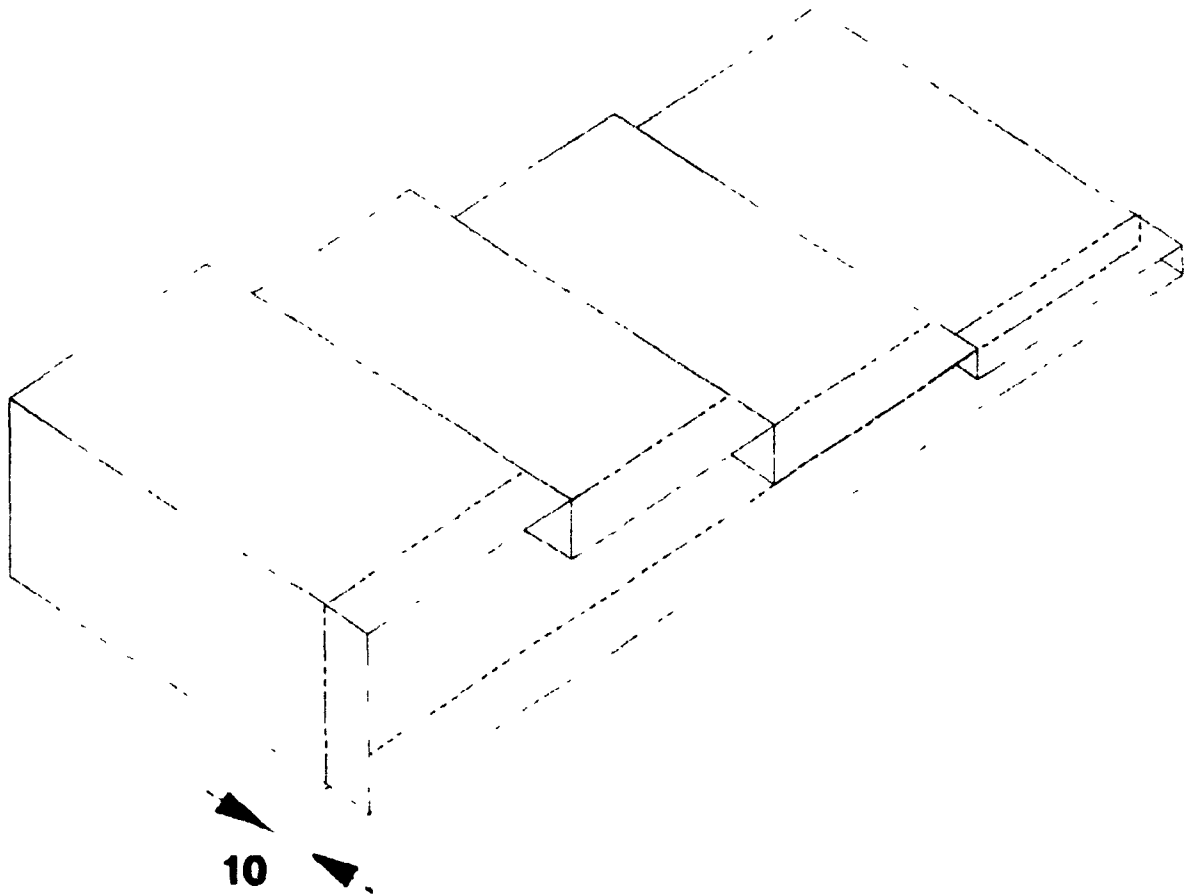


Figure 3.9 : Location of the metallographic samples

After mounting in bakelite, the samples were polished on a Leco automatic polishing machine. The procedure used was the following:

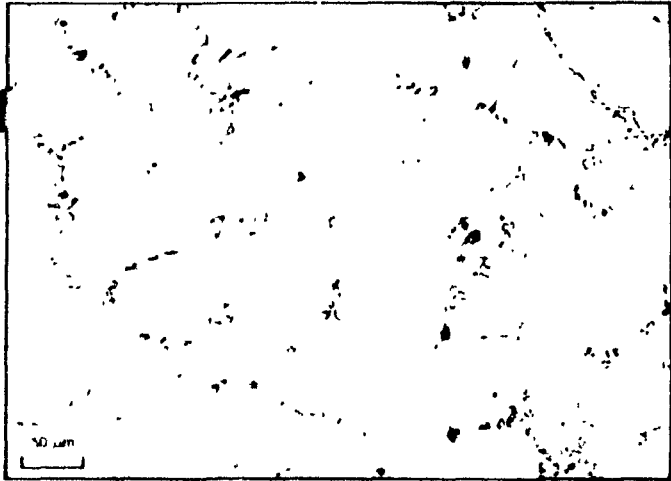
- grinding of the samples using successively 180, 400 and 600 grit silicon carbide papers and water as a lubricant on a high speed wheel.
- coarse mechanical polishing using a suspension of 5 micron alumina powder in water on a polishing cloth followed by a fine polishing with a suspension of 0.3 micron alumina.

- final mirror-like polishing using a solution of colloidal silica supplied by LECO Corp.

The polished samples were examined on a Neophot optical microscope primarily as polished for determination of the degree of modification. They were then etched in a solution of 0.5%HF, 0.5%HCl, 1%HNO₃ for 60 seconds and re-examined under the microscope for dendrite arm spacing measurement.

4.3 Determination of the degree of modification

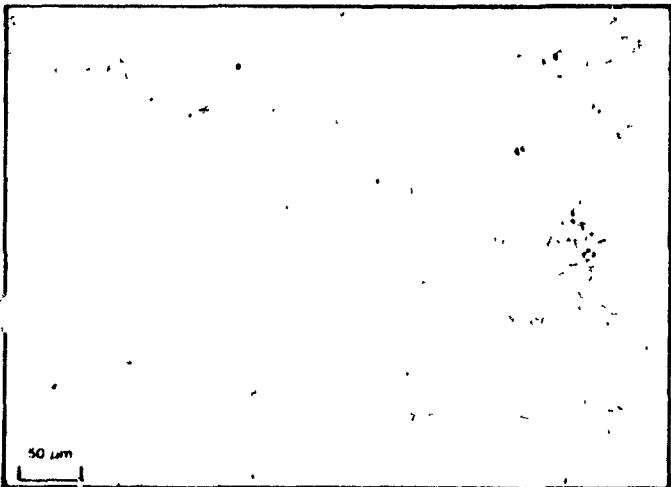
The degree of modification was evaluated from the standard grading system proposed by Sigworth et al. [61]. This grading system rates the silicon morphology according to six classes: (1) acicular, (2) coarse lamellar, (3) fine lamellar, (4) undermodified, (5) fibrous and (6) very fine fibrous (Fig. 3.10). A seventh class corresponding to an overmodified structure has recently been added. Ten areas of each sample were inspected and given a rating number. The average of the modification ratings was then taken as the global rating. Although not as precise a quantification method as image analysis, this method gives reliable results and can be readily used in a foundry.



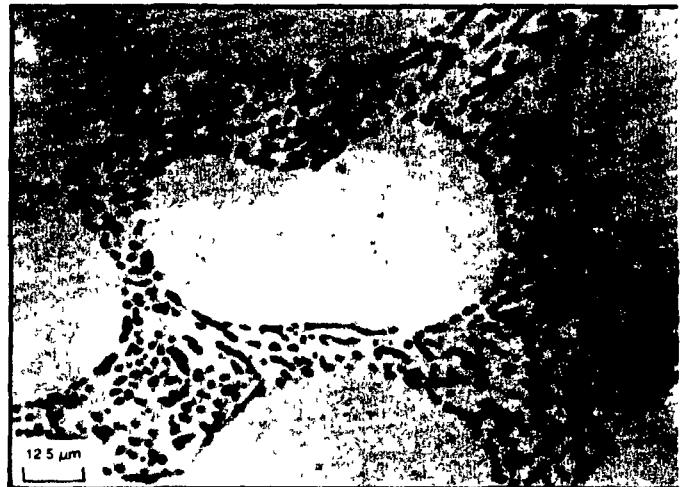
200x

Class 4 Absence of Lamellar Structure

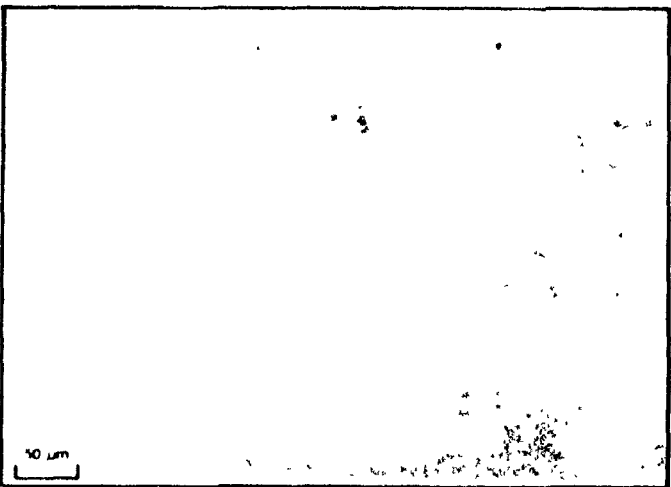
800x



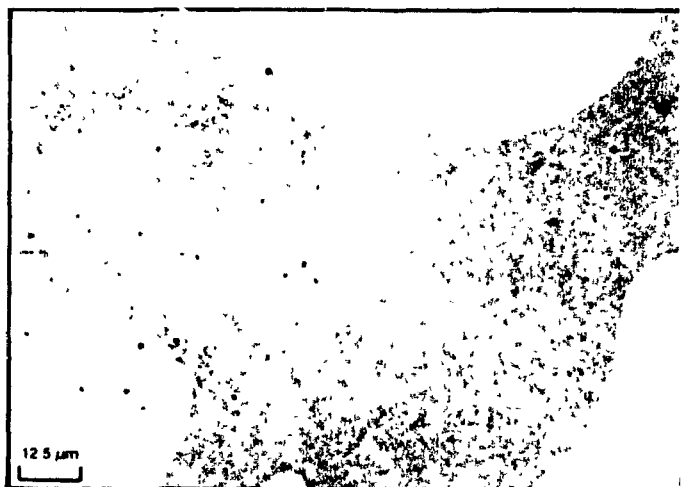
200x

Class 5 Fibrous Silicon Eutectic

800x



200x

Class 6 Very Fine Structure

800x

Figure 3.10 : Modification rating system [61]

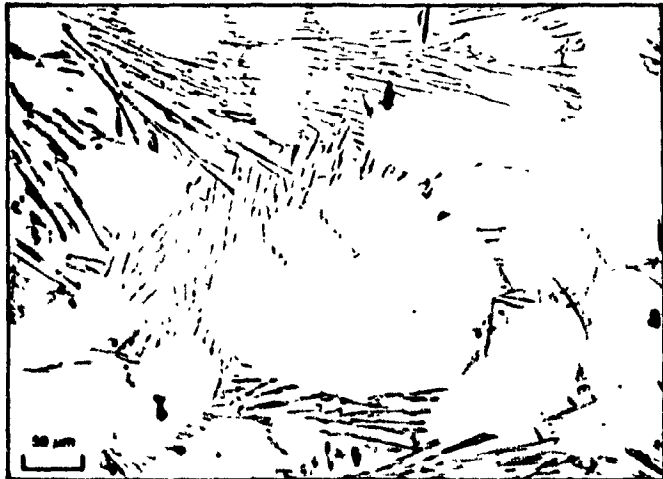


200x

Class 1 Fully Unmodified Structure



800x

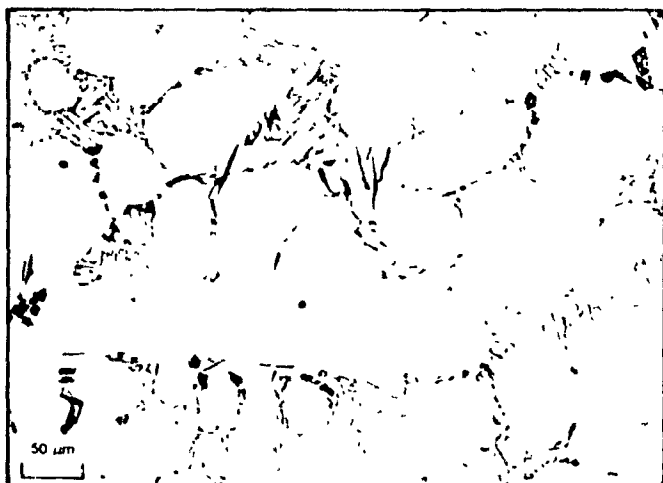


200x

Class 2 Lamellar Structure

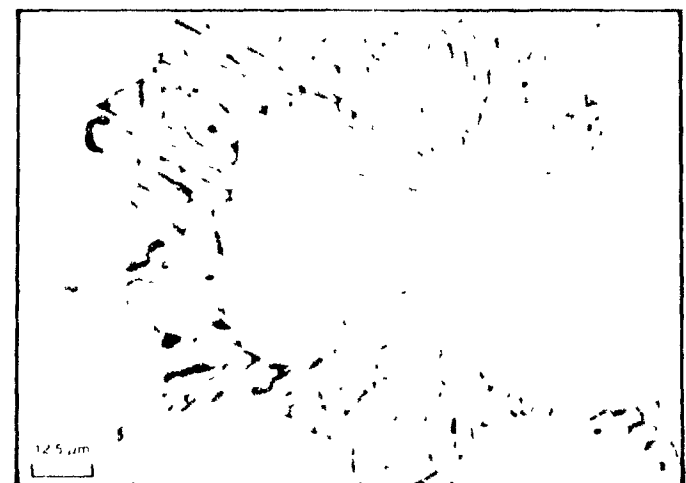


800x



200x

Class 3 Partial Modification



800x

Figure 3.10 : Modification rating system

4.4 Dendrite Arm Spacing

The Dendrite Arm Spacing (DAS) was measured by the line intercept method shown in Figure 3.11 on modified samples where the dendrites are well delineated. This method entails drawing a straight line perpendicular to the growth direction of the secondary dendrite arms and counting the number of intercepts of eutectic regions along the line. The DAS value is then determined by the relationship :

$$\text{DAS } (\mu\text{m}) = \frac{\text{Length of the intercept line (mm)}}{\text{Number of intercepts}} \times \frac{1000}{\text{Magnification}}$$

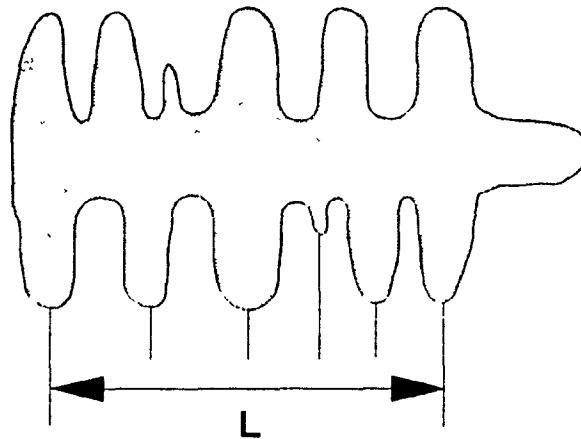


Figure 3.11 : DAS measurement technique

Ten measurements were taken on each step and the average calculated. For chill castings, the DAS was measured close to the top surface ie opposite to the surface in contact with the chill. The DAS could not, however, be determined on unmodified castings since the dendritic structure is not distinguishable from the overall microstructure (Fig.1.5). Hence, for unmodified castings, each step was ascribed a DAS value equal to the average of the DAS values measured on modified samples on corresponding steps.

This approximation is based on the following assumptions :

- The Mg content in the range 0-0.6% has a negligible influence on the solidification range. In other words, the introduction of small amounts of a ternary element (Mg) does not significantly shift the liquidus and binary Al-Si eutectic valley. Thus, the period of time spent in the interval of solidification, and during which dendrite coarsening occurs, is basically the same as for binary Al-Si alloy with an equivalent silicon concentration.
- the cooling rate at a given location in the mold was the same for each casting. This assumption is fairly realistic since the molten metal was always poured at 750°C in room temperature molds. In addition, the thickness of the coating on the aluminum chill was fairly constant.
- the eutectic temperature depression associated with modification, which indirectly increases the solidification range of modified alloys, has a negligible effect on dendrite arm spacing.

Statistical tests were carried out to verify that the DAS values measured on one step were not significantly different from one alloy to another. Statistical tests were also carried out to verify that the steps have significantly different DAS values.

4.5 Spectrochemical analysis

The chemical compositions of the castings were determined by optical emission spectrometry using samples cast in a copper mold. These samples were machined on their chilled surface before being analysed. The equipment used was a Baird Atomic Spectro 1000 model DV2 emission spectrometer. The standards used in the calibration of the spectrometer were supplied by Alusuisse Ltd. The results of the sample analyses are listed in Table 3.2.

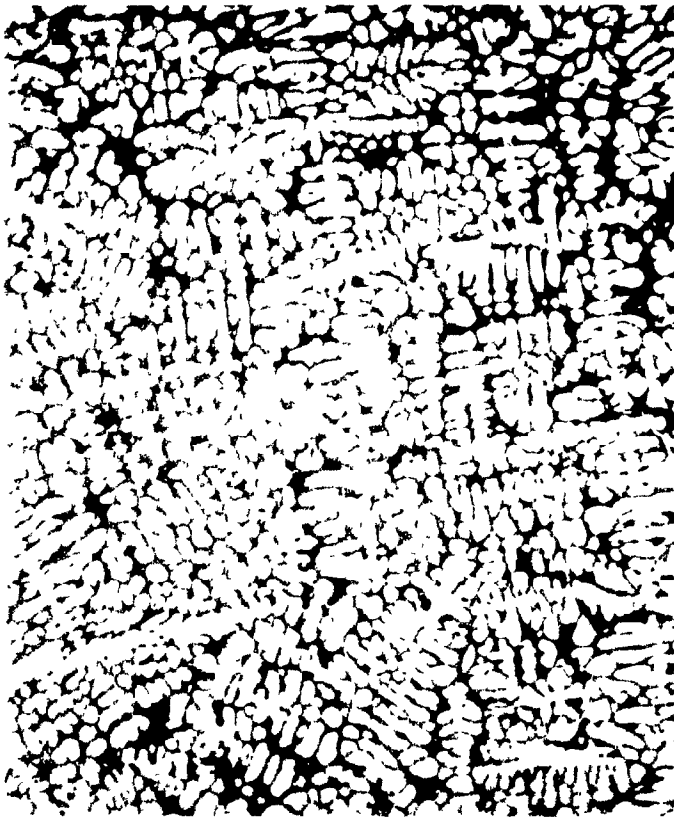
Alloy	%Si	%Fe	%Mg	%Ti	%Sr
A356A1	7.080	0.095	0.340	0.079	0.000
A356A6	7.160	0.082	0.380	0.080	0.000
A357A9	7.630	0.095	0.620	0.120	0.000
A356L8	7.610	0.076	0.410	0.078	0.014
A356M4	7.600	0.081	0.410	0.076	0.025
A356M10	7.700	0.074	0.420	0.078	0.032
A357F12	7.810	0.080	0.710	0.006	0.024
A357L11	7.580	0.084	0.710	0.006	0.001
SA3	7.760	0.110	0.000	0.080	0.000
SF7	7.970	0.100	0.000	0.120	0.027
SL5	8.080	0.110	0.000	0.120	0.006
A356M2	7.510	0.084	0.450	0.075	0.010
A1	7.870	0.100	0.000	0.130	0.000
SF14	7.630	0.137	0.000	0.005	0.027
A357A15	6.220	0.442	0.534	0.013	0.001

Table 3.2 : Chemical compositions of the melts

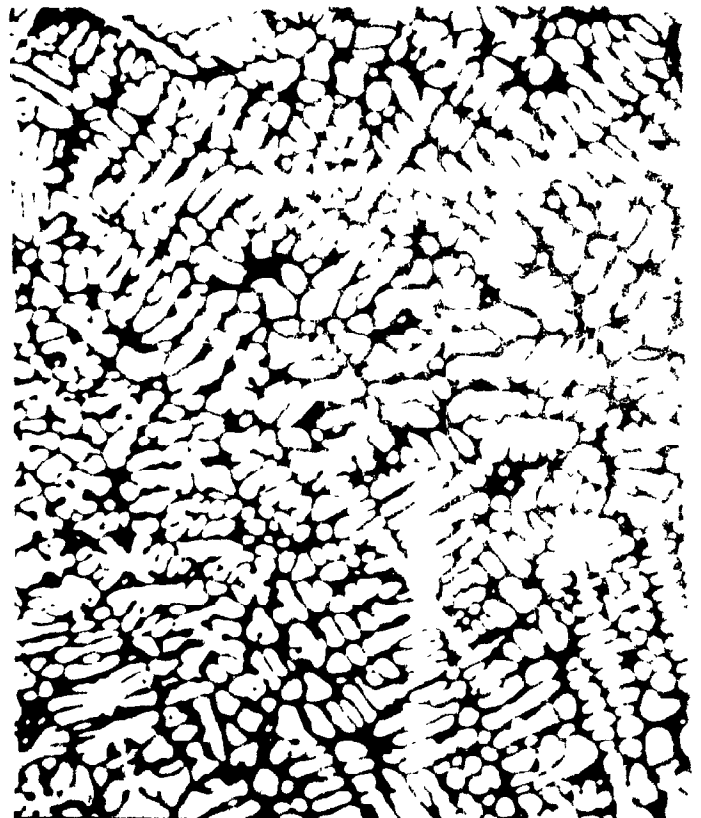
CHAPTER 4

RESULTS AND DISCUSSION

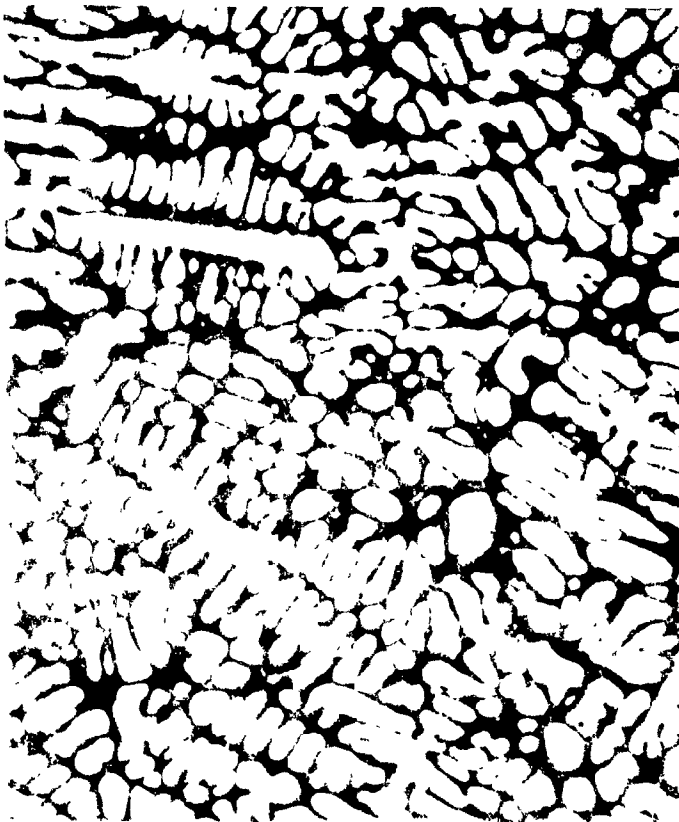
The DAS range covered in this study was 14-47 μ m. Figure 4.1 (a & b) shows typical micrographs of each step with the corresponding measured DAS.



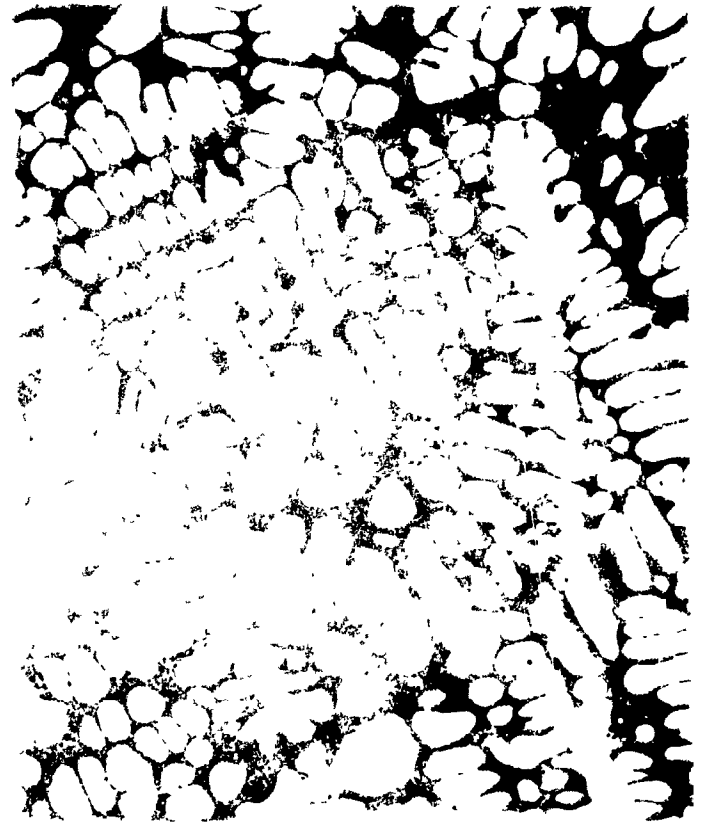
DAS = 13.5 μm



DAS = 17.3 μm

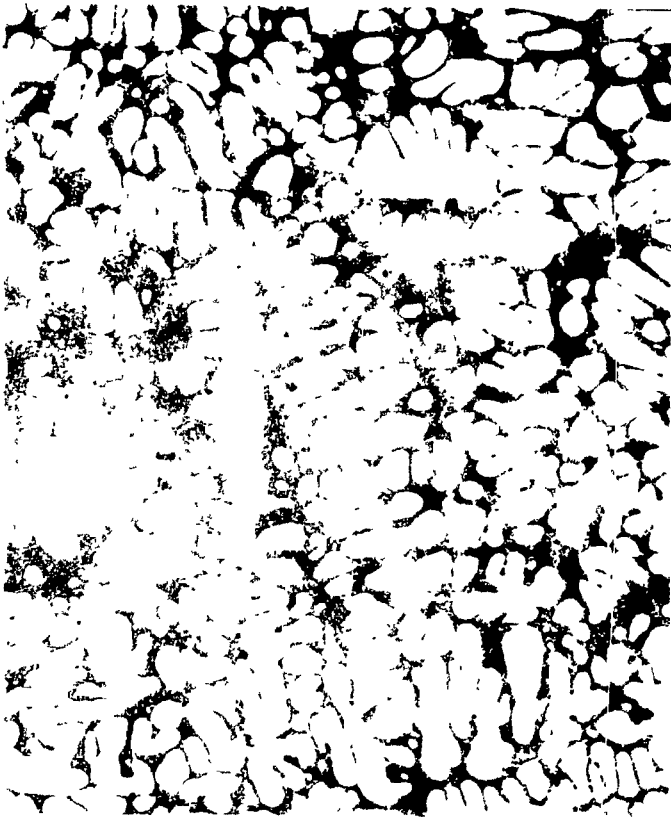


DAS = 20.4 μm



DAS = 28.7 μm

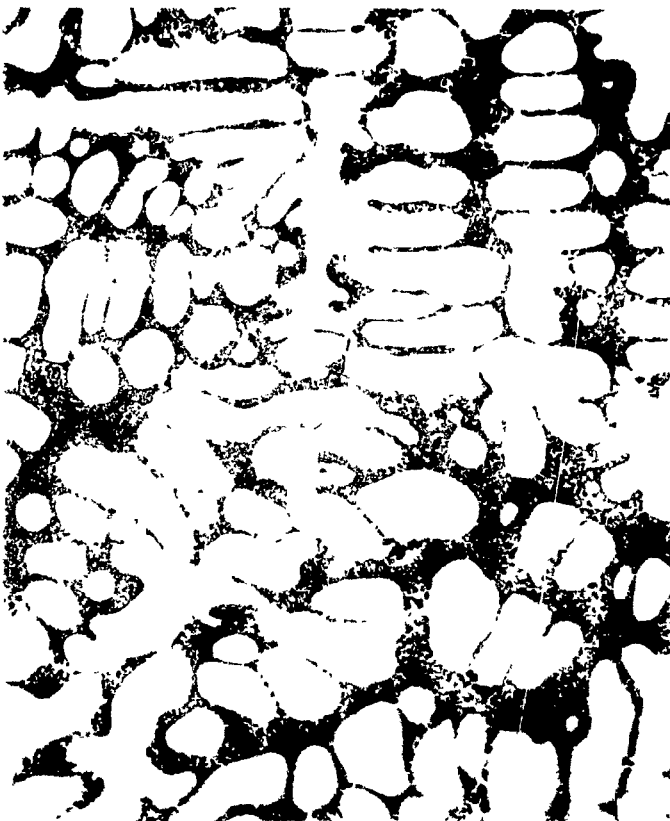
Figure 4.1 (a) : Micrographs showing the range of DAS covered (Chilled casting) Mag x 100



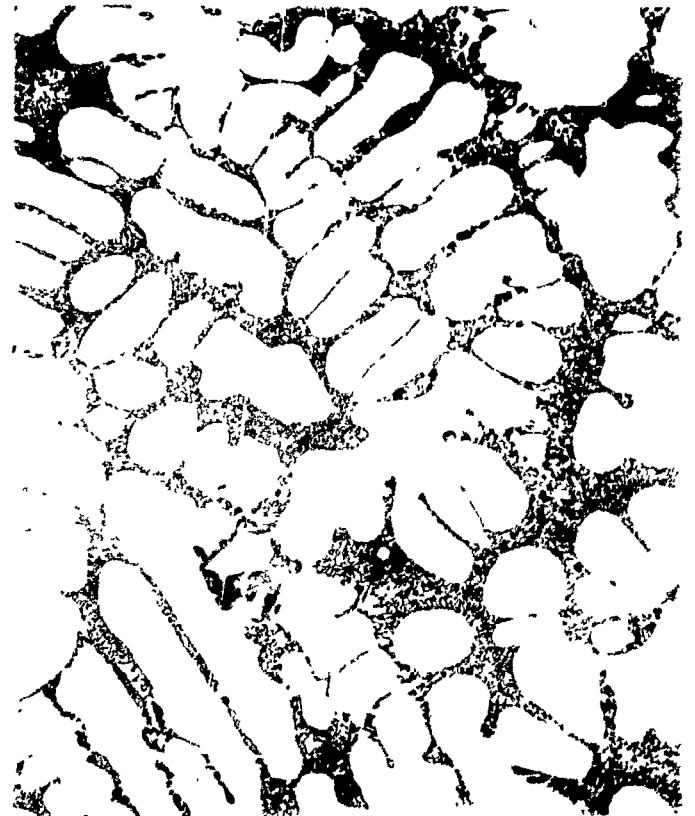
DAS = 24.3 μm



DAS = 31.5 μm



DAS = 40.9 μm



DAS = 48.3 μm

Figure 4.1 (b) : Micrographs showing the range of DAS covered (Unchilled casting)

1. AS CAST CONDUCTIVITY

1.1 Synthetic alloys

Experiments on synthetic Al-Si alloys were first carried out to investigate the effects of DAS and modification on the eddy current readout displayed by the K.J. Law eddy current tester. The eddy current readout displayed has no common units and varies with the frequency selected. As explained previously (chapter 3 § 4.1), when a frequency of 3 kHz is used, the readout depends only on the electrical conductivity of the material tested. Some correlations of the type :

$$\% \text{ IACS} = A \ln (\text{Eddy Current}) + B$$

where A and B are constants

have been established by Argo [16] using samples of known electrical conductivity.

However, since the purpose of this study was to evaluate the variation of electrical conductivity caused by either DAS or modification changes, it was decided not to convert eddy current readouts to electrical conductivity values expressed in % IACS. In the following discussion, the term conductivity therefore refers to eddy current readout.

Experiments on modified and unmodified melts were replicated at least once. Each type of symbol in the graphs that follow corresponds to a unique experiment. The eddy current measurements for modified and unmodified alloys are plotted as a function of DAS in Figure 4.2.

Conductivity values measured on chilled castings are represented by black symbols, whereas white symbols represent unchilled castings. The length of the error bars corresponds to the standard deviation of the measurements. The fitted curves are the second order polynomial interpolations calculated by the least squares method on the experimental results.

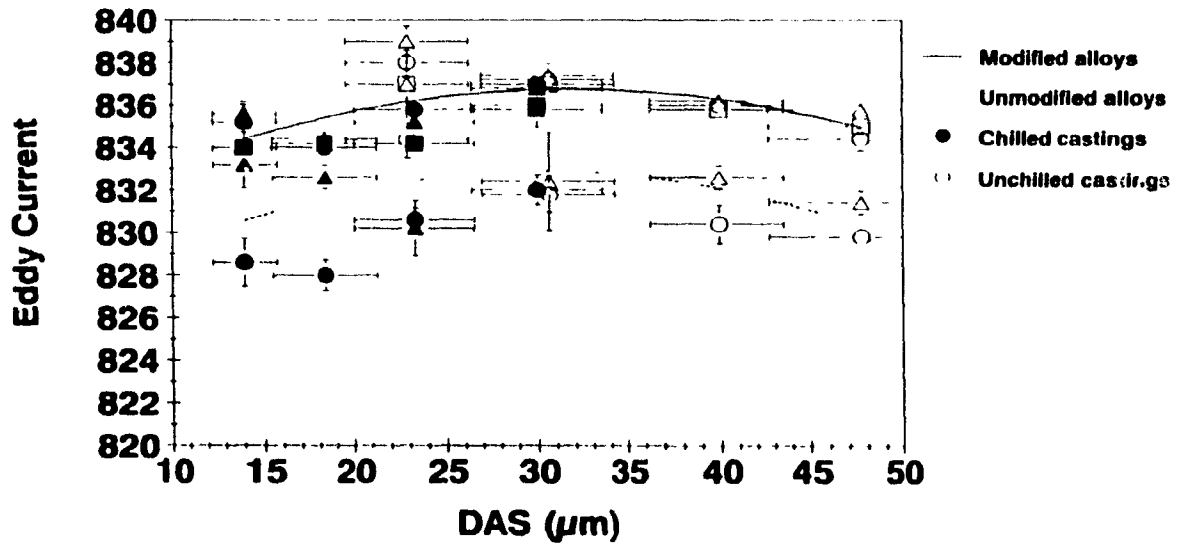


Figure 4.2 : Conductivity vs DAS plots for Al-Si binary alloy

It can be noted that :

- 1 : Electrical conductivity increases with modification, the increase being about 4 units of eddy current as the silicon morphology varies from acicular to fine fibrous.
- 2 : Considering exclusively measurements on unchilled castings (white symbols), electrical conductivity decreases approximately linearly as DAS increases independently of the level of modification.

- 3 : At DAS smaller than 30 μm , electrical conductivity measured on chilled castings decreases with decreasing DAS. Maximum conductivity is attained for a DAS of 30 μm .
- 4 : At DAS of 23 μm , chilled castings exhibit a conductivity which is lower than that of unchilled samples.
- 5 : Conductivity measurements from melt to melt are very reproducible; the maximum difference observed is 2 units. The apparently bad reproducibility at lower DAS values on unmodified alloys is attributable to a 0.05 % difference in the titanium concentrations of the two melts.

The observed increase in electrical conductivity with modification is in agreement with previous investigations [49,50,52]. This behaviour lies in the fact that the fine fibrous shape of the non-conductor silicon does not impede the electron flow as effectively as the coarse plate like form. Mulazimoglu [53] has shown in a very detailed study that, since electrons propagate exclusively in aluminum, the overall conductivity depends only on the projected surface between silicon particles and aluminum matrix which diminishes as modification of the alloy is achieved.

The linear conductivity decrease with DAS on unchilled castings is also in agreement with the results published by Argo et al. [16] on A356 alloy. However, unlike what these authors observed, the slopes of eddy current values versus DAS lines are the same for modified and unmodified Al-Si alloys.

At DAS of 23 and 30 μm chilled castings exhibit a lower conductivity which decreases with decreasing DAS. This is possibly due to the higher cooling rate after solidification generated by the aluminum chill. At high cooling rates, alloying elements in solid solution have less time to diffuse out of solid solution and remain in supersaturation at room temperature [37,40]. As reported in Chapter 2, alloying elements in solid solution impede more effectively the electron flow than do intermetallic compounds [28,50]: the overall conductivity of the alloy decreases as the degree of supersaturation of the solid solution increases. A graph published by Mulazimoglu [52] shows that the conductivity difference between modified and unmodified binary Al-Si alloys decreases when the solidification rate is increased from 0.4°C/s to 1°C/s . There is some indication that the same trend is observed at lower DAS on Figure 4.2.

1.2 A356 alloys

A356 alloys exhibit a conductivity behaviour similar to that of binary Al-Si synthetic alloys as seen in Figure 4.3 :

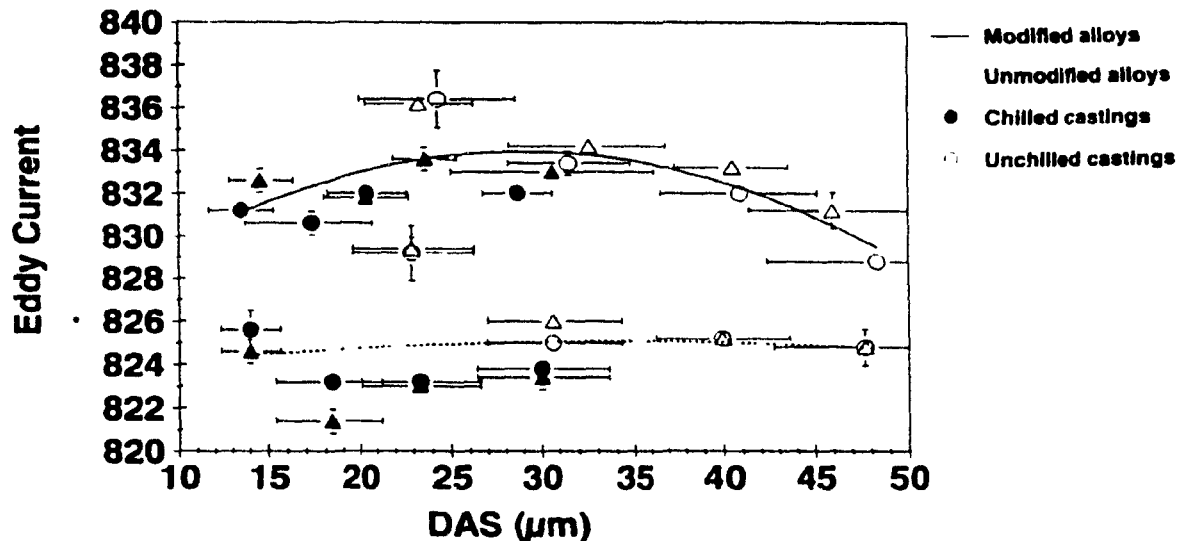


Figure 4.3 : Conductivity vs DAS plots for A356 alloy

- 1 : Modified alloys show a higher conductivity than unmodified ones. The difference which varies from 5 to 10 units is more important than for binary alloys.
- 2 : The relation between conductivity and DAS is linear for unchilled castings, but, unlike binary Al-Si alloys, the slope of the line increases when the alloys are modified. These results are in total agreement with those of Argo and Gruzleski [16] as long as chilled castings are not taken into account.
- 3 : On unmodified alloys, there is no noticeable effect of DAS on electrical conductivity. This is attributable to the coarse microstructure of unmodified alloys in which dendrite arms are not well delineated (Fig. 1.5.b). In modified alloys, on the contrary, well developed pockets of eutectic structure delineate the dendritic network (Fig. 1.5.a), and therefore changes in dendrite arm spacing yield higher conductivity variations than do changes when the structure is unmodified.
- 4 : Electrical conductivity of chilled castings decrease with decreasing DAS owing to a higher cooling rate in the solid state which restrains the diffusion time and leads to a supersaturated solid solution.
- 5 : As for binary alloys, the reproducibility of the measurements is good , and the differences from melt to melt for a fixed DAS are of the order of 2 units of eddy current. The small variability is indicative of the accuracy of the eddy current technique.

However, due to the parabolic shape of the regression curves, an uncertainty of 2 units on the conductivity results in a prediction of DAS with an accuracy of 25 μm . This is, of course, unacceptable.

Finally, the results on the as cast samples can be summarized as follows :

- Electrical conductivity of an alloy increases with modification
- Conductivity decreases with increasing DAS in the range 30 μm - 50 μm , and the effect is more pronounced with modified alloys.
- At DAS values lower than 30 μm , precipitation in the solid state becomes important and overcomes the effect of DAS on conductivity.
- Conductivity measurements are reproducible from melt to melt within a 2 units variation.

1.3 Calculation of polynomial model fitting the experimental results

Although the technique may not be of great interest in industrial practice, a second order polynomial model was fitted to the experimental results. A model helps identify the factors influencing the electrical conductivity of an alloy and determine the importance of their effect. Prior to the calculation, measurements were standardized, that is actual values were replaced by standard values defined as : (real value - average of the values)/standard deviation. The use of standard values increases the accuracy of the calculation by suppressing the correlation between first and second order terms. The results of the calculations are listed in Table 4.1.

Independent variables	Coefficient	Standard error
Constant	832.68	0.33
DAS	0.42	0.19
Structure(modification)	2.72	0.20
Ti	- 2.30	0.22
Mg	- 3.05	0.23
Fe	- 1.87	0.19
Structure ²	- 0.75	0.23
DAS ²	- 0.84	0.17
$R^2 = 0.88$		

Table 4.1 : Coefficients of the polynomial model

The sign of a coefficient is indicative of the effect of the associated factor on conductivity while the coefficient itself represents the importance of the factor. Calculations show that alloying elements like magnesium, titanium and iron have a negative effect and therefore lower electrical conductivity. This is accounted for by the distortion of the crystal lattice by dissolved atoms of different atom radii which makes the electron flow more difficult [19,23]. Consequently, the impurity component of resistivity is increased and the overall conductivity drops. According to the values published by Fickett [18], titanium and iron affect very effectively the conductivity of aluminum whereas magnesium has a smaller effect. In this study, the computed coefficient of magnesium is higher than that of titanium and iron. This results from the use of standard values and the higher range of variations of the magnesium content in the experiments: a 1% change in the magnesium content is not equivalent to a 1% change in the titanium or iron contents since the standard deviation of each element is different.

Dendrite arm spacing and modification both have a second order influence on conductivity. As seen on the response surface and contour plot respectively in Figures 4.4 and 4.5. The rate of conductivity increase with modification is maximum when the alloy is not modified, but progressively decreases as the modification rating increases. Hence, a change in silicon morphology from coarse plate to fine lamellar causes a higher increase in conductivity than does a further change from fine lamellar to fine fibres. Figure 4.5 represents the iso-conductivity lines as a function of DAS and modification rating.

It could be used in industrial practice to determine the level of modification of a melt prior to pouring. The procedure would involve the three following steps :

- 1 : Casting of a sample in a mould yielding a constant and known solidification rate (i.e constant DAS).
- 2 : Measurement of the electrical conductivity of the sample cooled down to room temperature.
- 3 : Use of Figure 4.5 to determine the potential level of modification of the melt located on the graph at the intersection of the line of constant DAS with that of the measured conductivity.

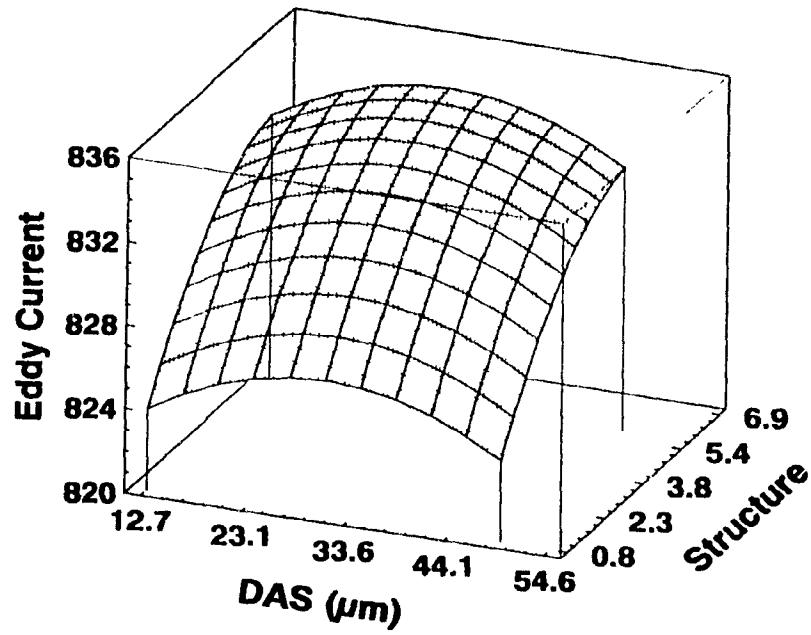


Figure 4.4 : Polynomial model response surface

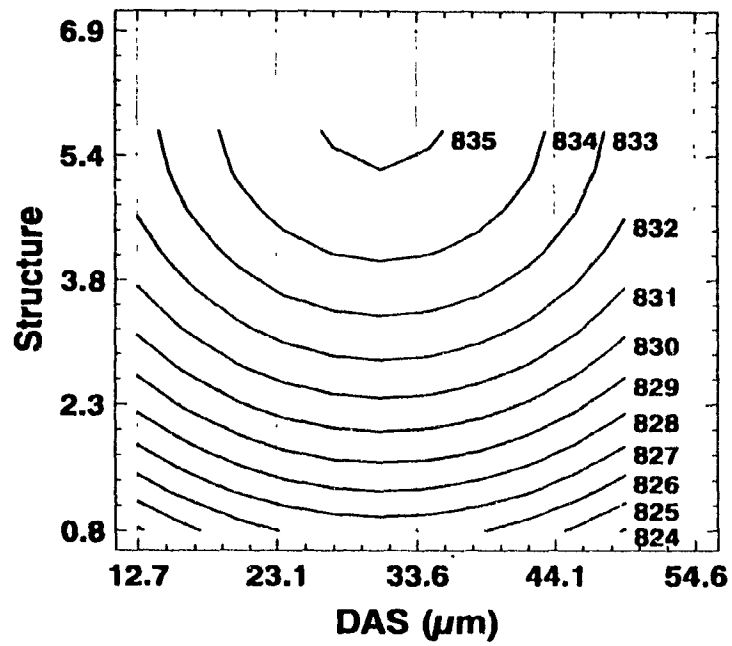


Figure 4.5 : Polynomial model contour plot

However, since the rate of conductivity change decreases when the silicon morphology becomes finer, the method may lack accuracy to differentiate an undermodified alloy from a well modified one.

It has been observed that the shape of the conductivity versus DAS curve changes with modification. However, the fitted polynomial model contains no DAS* Modification interaction term, and therefore does not represent exactly the conductivity changes observed.

2. INFLUENCE OF A PRECIPITATION TREATMENT

In order to verify whether the lower conductivity at low DAS is due to a retention of alloying elements in solid solution, precipitation treatments involving an artificial aging at 200°C for 4 hours were carried out on some of the samples. The purpose of the precipitation treatment was to enable alloying atoms in solid solution to diffuse and form precipitates so as to obtain a relatively homogeneous aluminum matrix whatever the chilling of the casting. In the experiments, chilled and unchilled castings made from the same melt were placed together inside the heat treatment furnace.

2.1 Al-Si synthetic alloys

Conductivity values in as cast condition and after the precipitation treatment are plotted in Figure 4.6. As seen, the conductivity of binary Al-Si alloys was not influenced by the treatment. It is likely that the temperature at which the treatment was performed was too low for silicon atoms to diffuse, and the aluminum solid solution thus remained supersaturated.

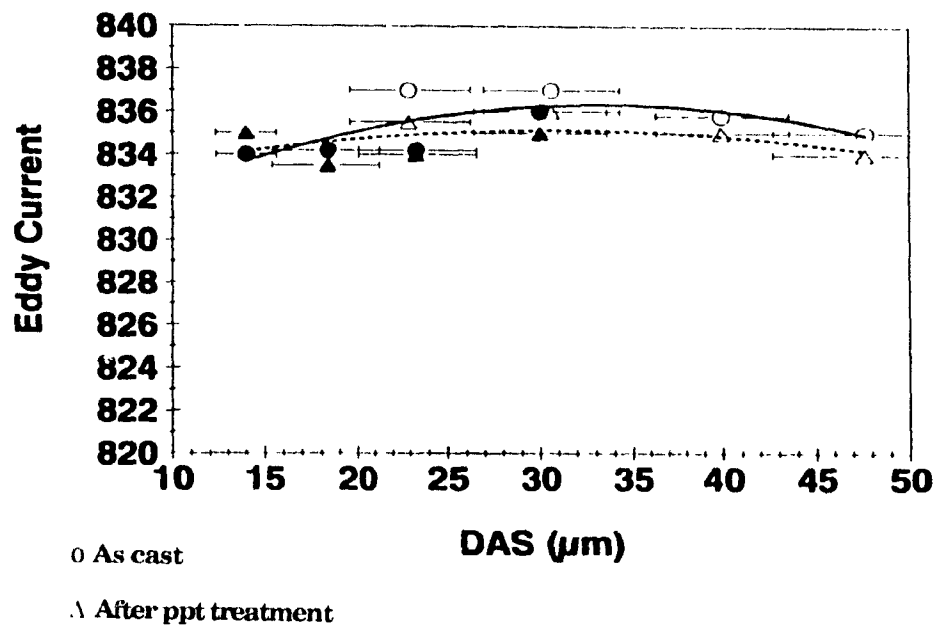


Figure 4.6 : Conductivity vs DAS plot for Al-Si binary alloy after precipitation treatment (8 hours at 155°C)

After the precipitation treatment, a metallographic analysis of the castings indicated that the morphology of the eutectic silicon had not been altered by the treatment.

2.2 **A356 alloys**

Figure 4.7 shows the change in electrical conductivity with DAS variations for as-cast samples and after a precipitation treatment of 8 hours at 155°C. As seen, heat treated samples exhibit a higher electrical conductivity than in the as-cast condition. This has been investigated in the past and is known to arise from the formation of precipitates of Mg_2Si which do not impede the electron flow as effectively as atoms of magnesium and silicon in solid solution [55]. In addition, it is observed that :

- on each step of the unchilled casting, conductivity has increased by the same value; the conductivity versus DAS line is simply shifted to higher conductivities. This was reported in a previous study by Argo and coworkers [16].

- Conductivity changes after the precipitation treatment on chilled casting are maximum on the thinnest step and decrease as DAS increases. This tends to confirm the validity of the hypothesis that more alloying elements are retained in solid solution in chilled castings in the as-cast state because of a higher cooling rate after solidification. The effect of the heat treatment is to enable the diffusion of alloying elements in the matrix until the equilibrium composition is reached. The higher the supersaturation of the matrix, the longer diffusion and precipitation processes will proceed. Therefore, the precipitation phenomenon is more important in a supersaturated alloy than in a near equilibrium one, and so is the conductivity change.

The regression curve becomes linear after the precipitation treatment. However, above 30 μm , conductivity changes with DAS are very small so that the technique may not be accurate enough to predict DAS change in this range.

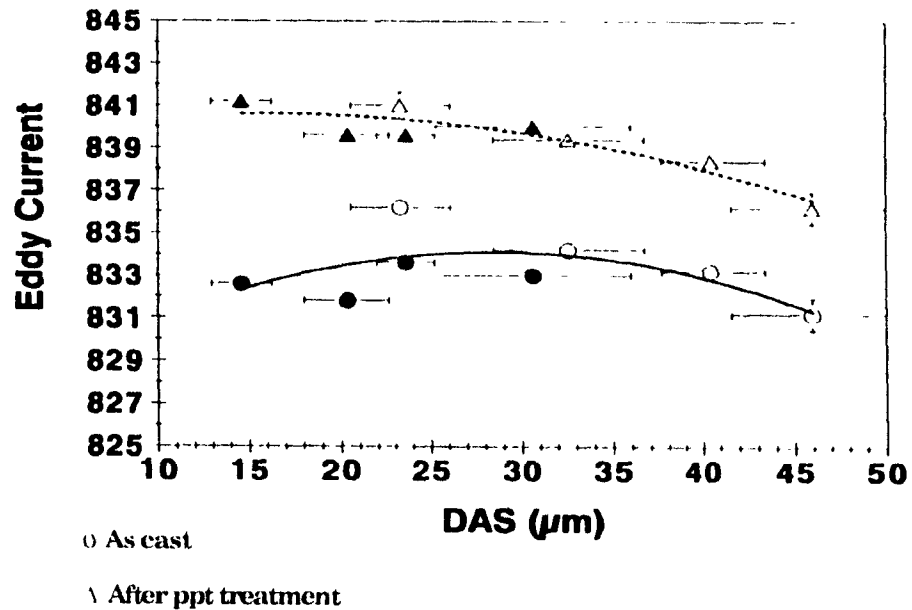


Figure 4.7: Conductivity vs DAS plot for A356 alloy after precipitation treatment (8 hours at 155 °C)

To conclude, it has been shown that :

- 1: DAS determination by electrical conductivity measurement requires that the aluminum matrix be homogeneous.
- 2: a precipitation treatment improves the matrix homogeneity of A356 alloys, and consequently the accuracy of the determination, but the technique still lacks accuracy at DAS larger than 30 μm

3. HEAT TREATMENT

Although a precipitation treatment improves the conductivity response to DAS changes by rendering the matrix more homogeneous, it is not a common foundry practice, and so cannot be considered seriously as it will increase the manufacturing cost of the castings. For this reason, an industrial heat treatment consisting of a solution treatment at 540°C for 10 hours, followed by a rapid quenching in cold water and an artificial aging at 160°C for 6 hours, was carried out on the samples. Such a treatment has the beneficial effect of homogenizing the aluminum matrix, but spheroidization of the eutectic silicon also occurs in the solution treatment phase [32], and the resulting structure is therefore different from that in the as cast state.

Conductivity measurements for each alloy after the heat treatment are represented on 2 graphs : the experimental measurements are plotted on the upper graph whereas the lower graph shows the second order polynomial curves calculated by the least squares method on the measurements.

3.1 Al-Si synthetic alloys

3.11 Unmodified alloy

Results on unmodified Al-Si synthetic alloys are plotted in Figure 4.8. The plots show that :

- 1: After the heat treatment, conductivity decreases with increasing DAS over the whole range investigated. Hence, heat treating the castings results in an improvement of the conductivity response to DAS change.
- 2: When DAS exceeds $30\ \mu\text{m}$, the electrical conductivity versus DAS curve becomes asymptotic so that changes in DAS fall below the limit of detectability of the method.
- 3: Electrical conductivity increases at small DAS ($<22\ \mu\text{m}$), but decreases for higher DAS with respect to as-cast values.
- 4: T4 and T6 conductivities are identical for all DAS.

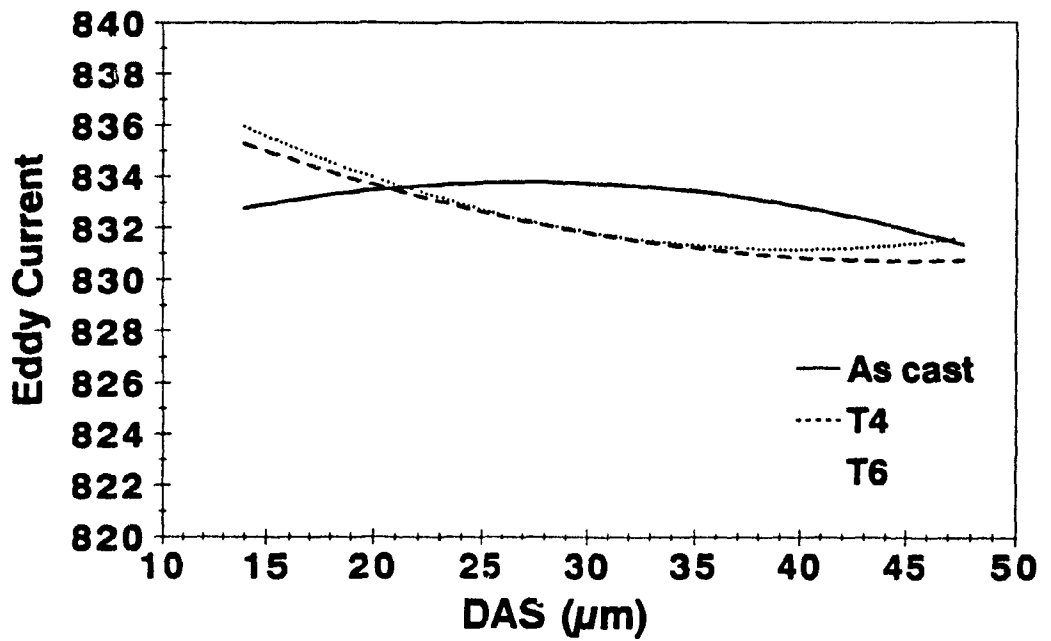
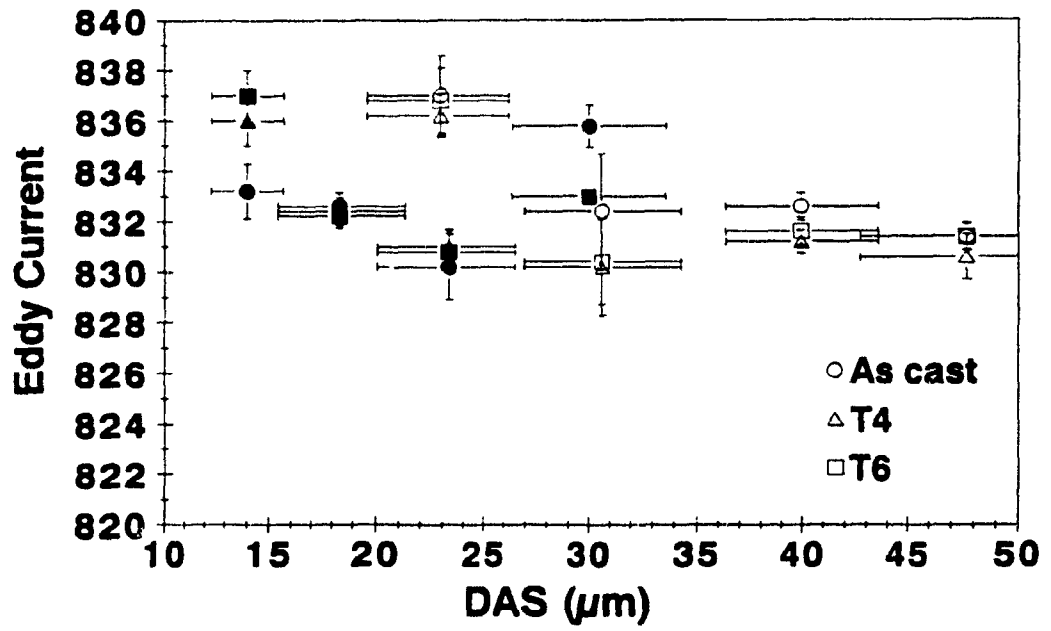


Figure 4.8 : Conductivity vs DAS plots for unmodified Al-Si alloy.
(As cast, T4 & T6 conditions)

3.12 Modified synthetic alloy

The shape of the electrical conductivity versus DAS plot for Al-Si modified alloys after heat treatment is very similar to that of unmodified alloys as seen in Figure 4.9. The drop in conductivity is, however, more important for modified alloys. In addition, electrical conductivity after heat treatment is lower than as cast conductivity in the whole range of DAS.

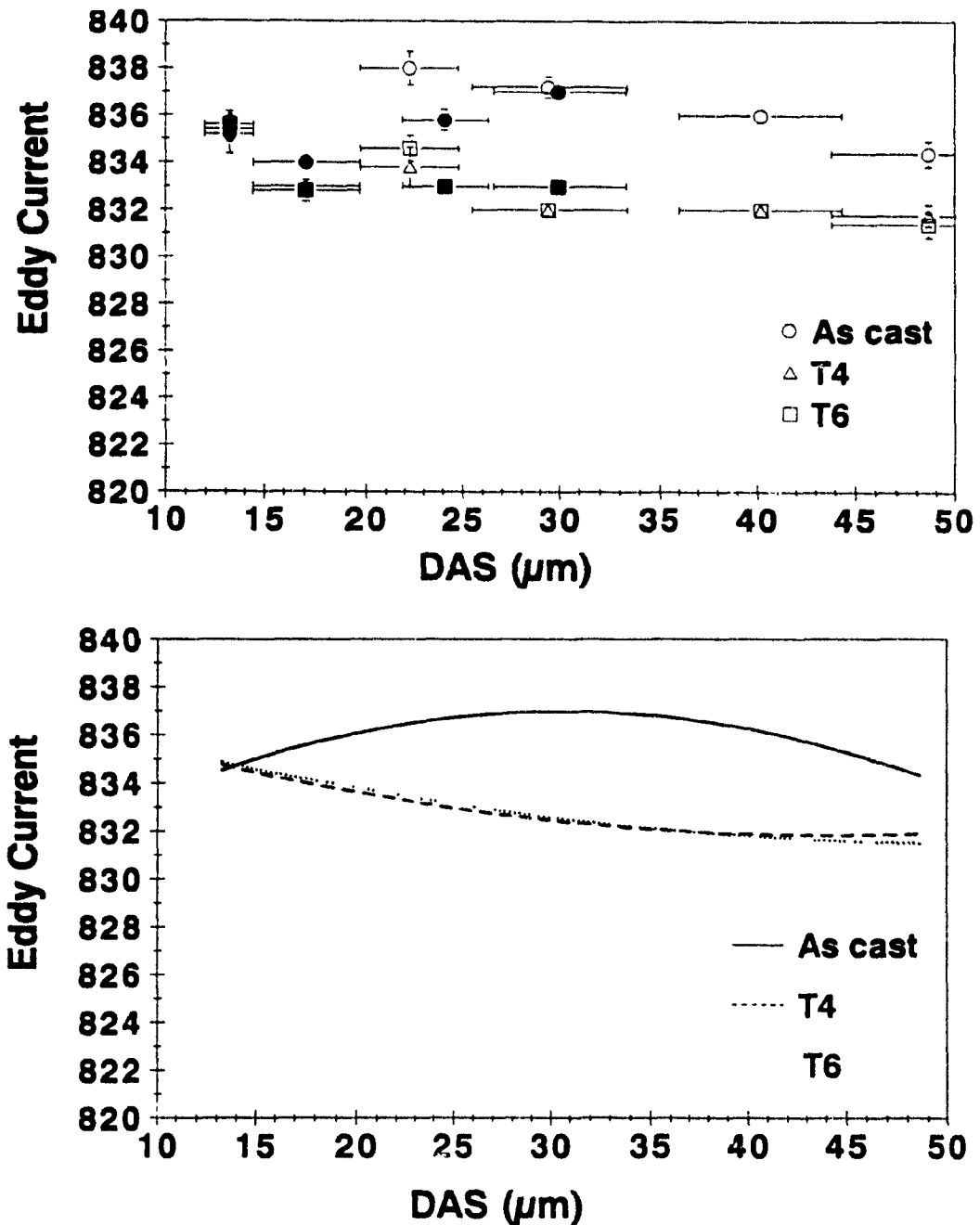


Figure 4.9 : Conductivity vs DAS plots for modified Al-Si alloy (As cast, T4 & T6 conditions)

3.2 A356 alloy

3.21 Unmodified alloy

The improvement of the conductivity response to DAS changes upon heat treatment is shown in Figure 4.10. Like the Al-Si synthetic alloy, the conductivity-DAS relationship after heat treatment becomes approximately linear, but the slope of the line, and so the accuracy of the method, are higher. For this alloy, conductivity increases after heat treatment for DAS lower than 35 μm but decreases for higher DAS. As compared to binary alloys, the DAS range within which conductivity is increased by a heat treatment is wider for Mg containing A356 alloys. This is probably related to the differences in the microstructures of these two alloys as shown in Figure 4.11.

It is worth noting that artificial aging (T6) promoted changes in the T4 conductivities unlike what was observed on binary synthetic alloys.

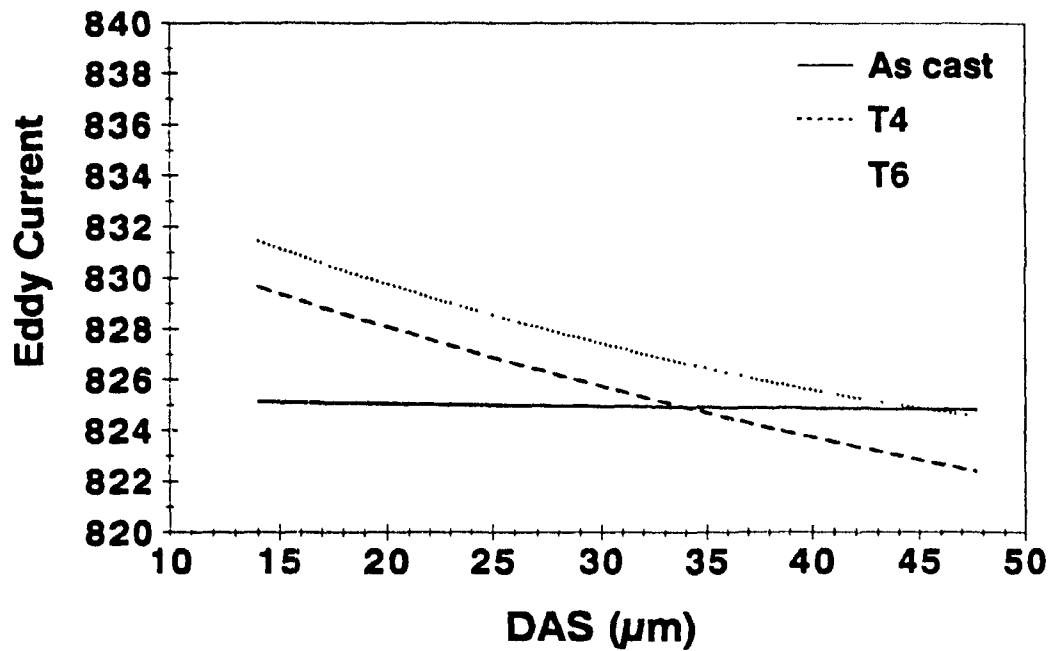
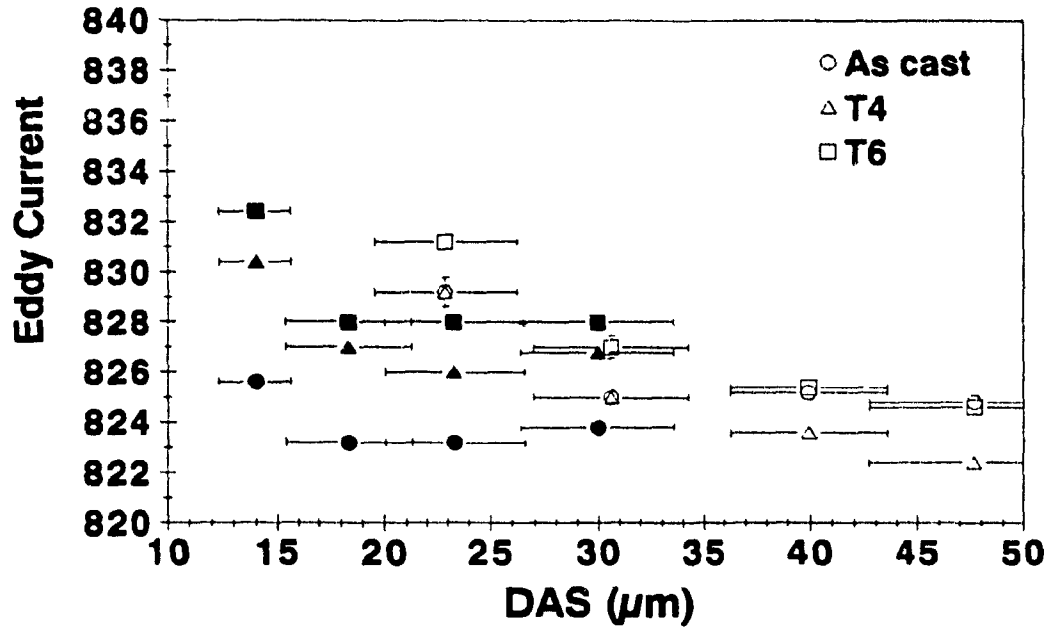


***Figure 4.10: Conductivity vs DAS plots for unmodified A356 alloy
(As cast, T4 & T6 conditions)***



A356 alloy

Synthetic Al-Si alloy

Figure 4.11 : Micrographs of as cast unmodified synthetic Al-Si and A356 alloys. Mag.X150

3.22 Modified alloy

The conductivity behaviour of modified A356 alloy during heat treatment is very similar to that of modified synthetic alloy (Fig. 4.12).

Heat treatment leads to a drop of electrical conductivity over the whole range of DAS investigated, but, at lower DAS, conductivity was not affected by the treatment. The eddy current versus DAS regression lines after heat treatment appear to be more linear than those of Al-Si synthetic alloys (Fig. 4.9).

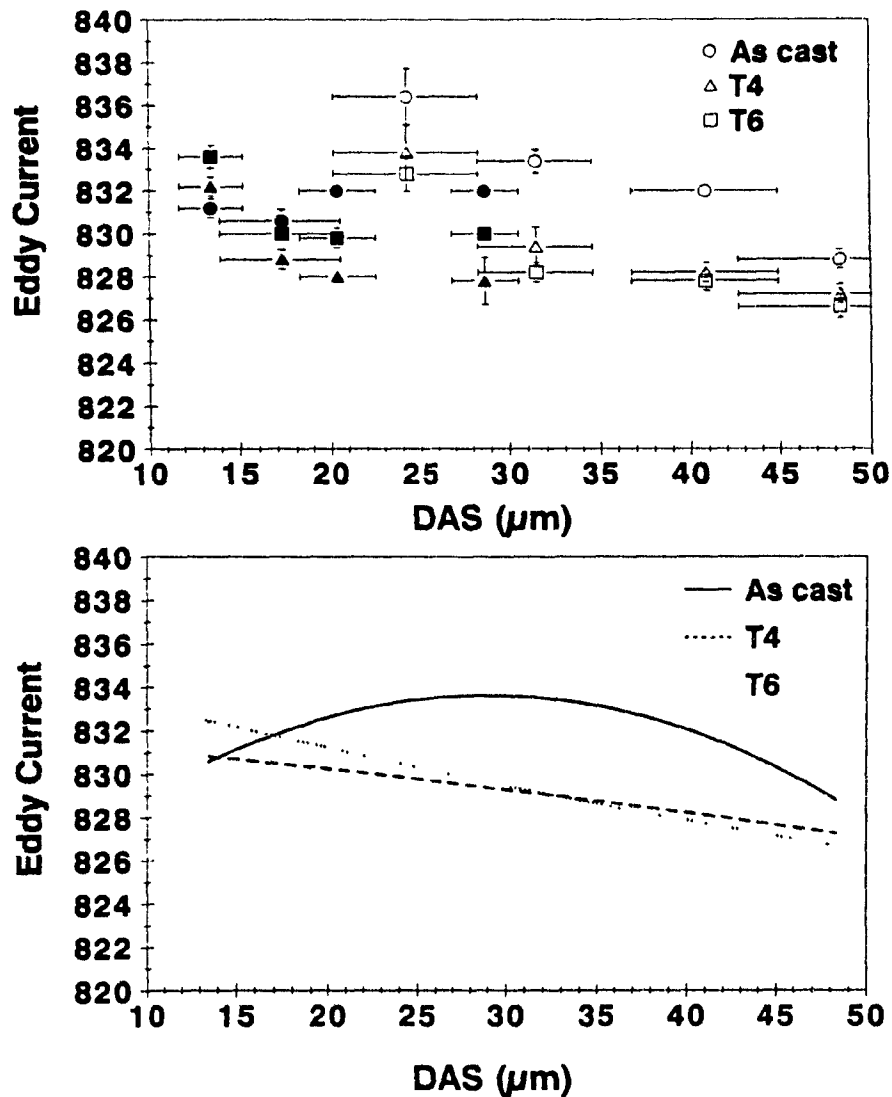


Figure 4.12 : Conductivity vs DAS plots for modified A356 alloy

(As cast, T4 & T6 conditions)

It can also be noticed that the precipitation treatment did not significantly change the conductivity although higher values in the T6 condition were expected. Similar results were obtained by Closset [55] who reported a 1-2% increase in resistivity for unmodified A356 compared to a 8-9% for modified A356 after a solution treatment carried out at 540°C for 8 hours.

4. DISCUSSION

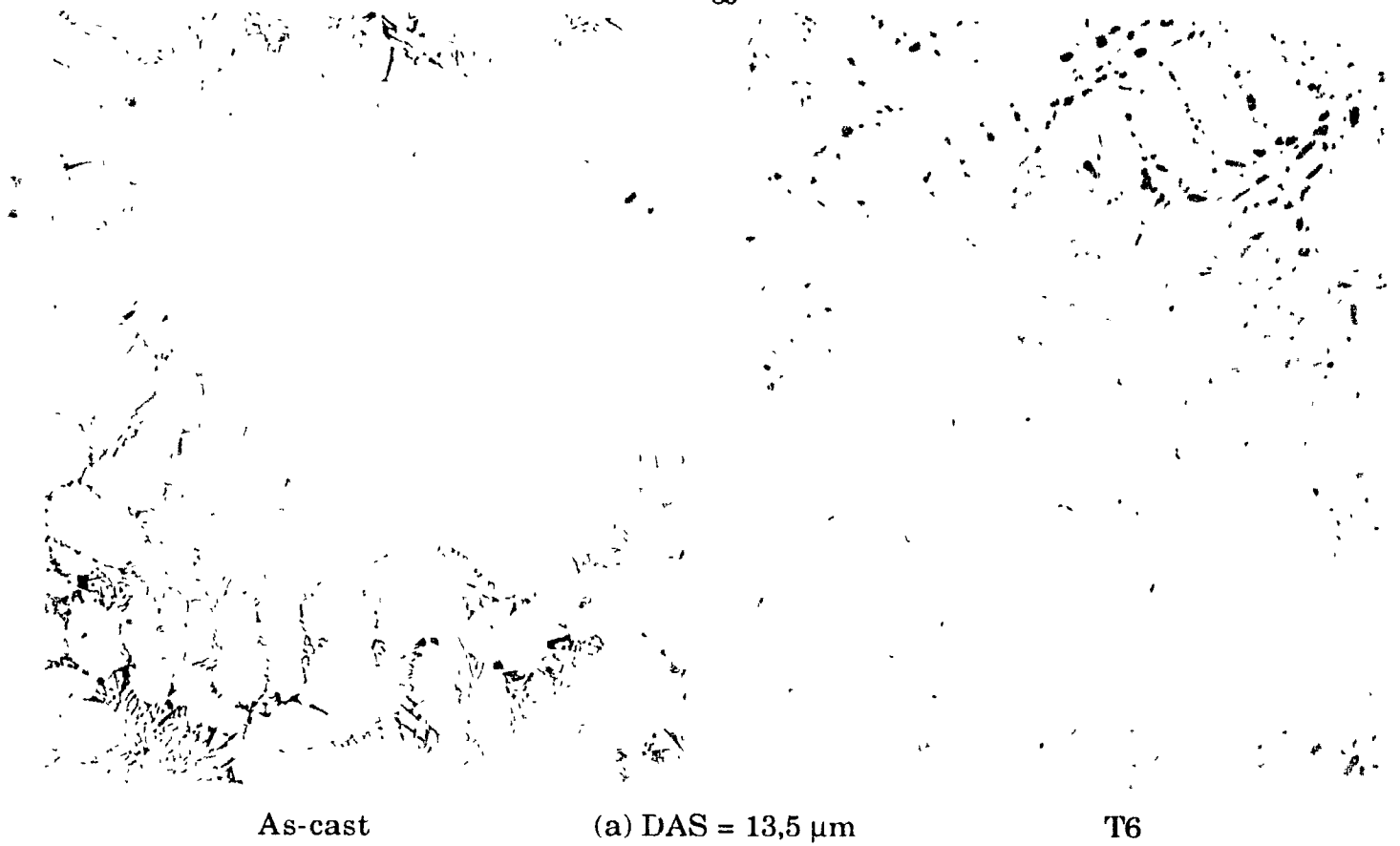
As was mentioned in Chapter 2, electrical conductivity changes upon heat treatment result from the two following microstructural changes which occur at high temperature :

- Dissolution of intermetallic compounds into the matrix which is due to the increase in solubility in the matrix with increasing temperature. This process proceeds until equilibrium composition at the treatment temperature is reached. The matrix becomes supersaturated at room temperature after quenching in cold water. This phenomenon increases the impurity term of electrical resistivity, and consequently decreases the conductivity of the alloy [28]. Mulazimoglu [53,57] has shown that dissolution is complete after 3 hours

- Spheroidization and coarsening of eutectic silicon particles driven by a system tendency to reduce its interfacial energy. As silicon particle spheroidize and coarsen, the interfacial area between eutectic particles and the aluminum matrix decreases. Consequently, the ability of electrons to flow through the metal improves, and the overall conductivity of the alloy increases.

It has been established that the rate of spheroidization and coarsening is inversely proportional to the silicon particle size [56,57] ; fine fibrous silicon particles spheroidize faster than coarser plate-like silicon. Therefore, unmodified and modified alloys behave differently during solution treatment with regard to silicon morphology changes, and so do castings of different DAS whose microstructures are more or less refined.

Figures 4.13 and 4.14 show the microstructures of Al-Si modified and unmodified alloys solidified at different cooling rates in the as cast and T6 conditions. As seen, after the heat treatment, spheroidization is complete for the modified alloy while elongated particles remain in the unmodified alloy of higher DAS. Thus, microstructural changes being considered, the conductivity changes during heat treatment may be explained as follows.



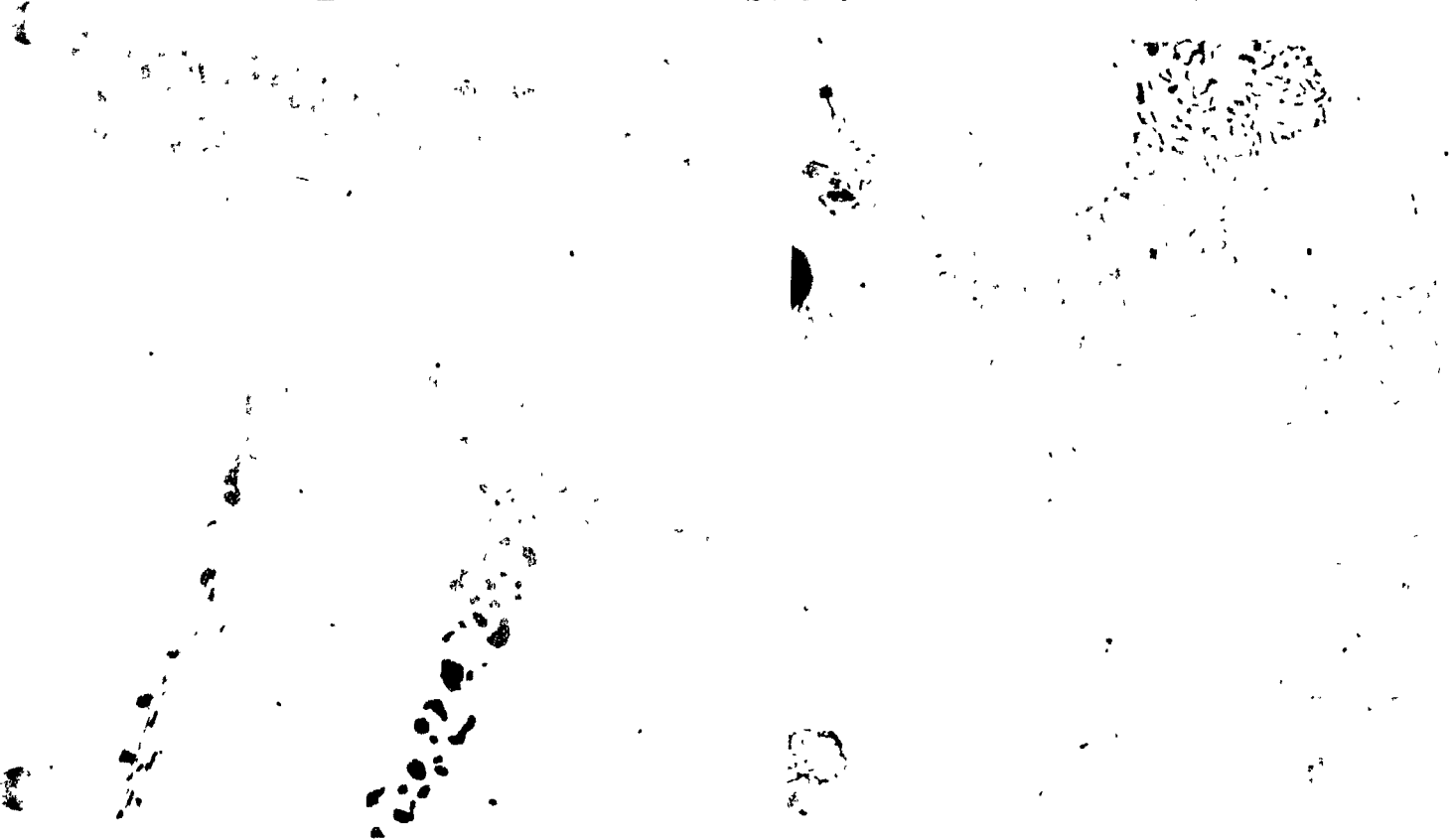
***Figure 4.13 : Micrographs of as cast and T6 unmodified Al-Si alloy
at two different DAS. Mag : X 500***

Figure 4.14: Micrographs of as cast and T6 modified A356 alloy

As-cast

(b) DAS = 48,3 μm

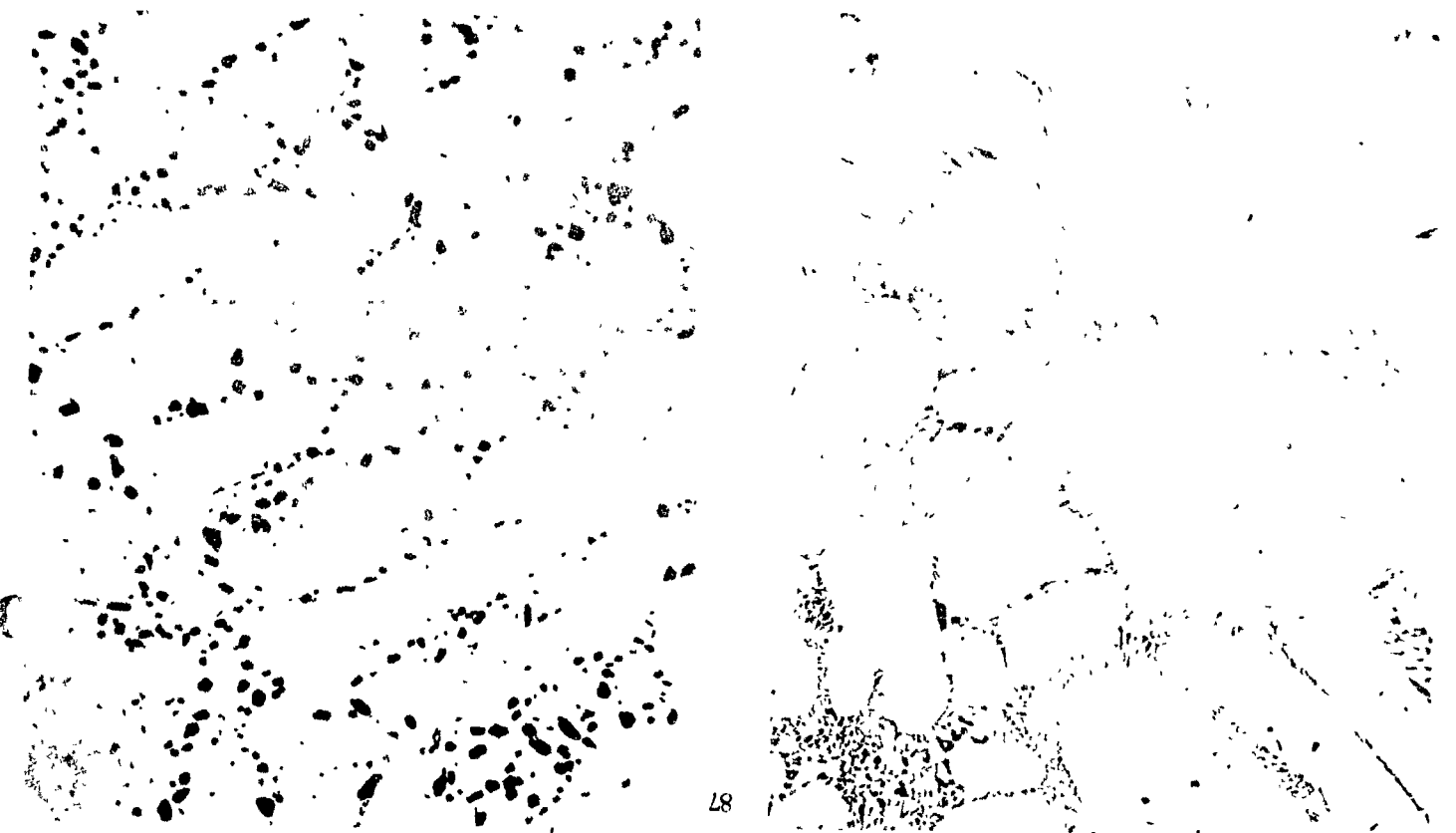
T6



As-cast

(a) DAS = 13,5 μm

T6



4.1 Unmodified Al-Si alloy

At lower DAS, the high cooling rate produced by the chill yielded a partially supersaturated aluminum solid solution in the as cast state. Consequently, fewer atoms need to dissolve into the matrix for equilibrium composition at 540°C to be reached, and the dissolution process rapidly reaches completion. The resulting conductivity decrease is therefore minor. Conversely, the rate of spheroidization is high since the as cast structure is fine (Fig. 4.13 a), and the silicon particles spheroidize completely. Hence, the increase in conductivity due to spheroidization and coarsening overcomes the small decrease associated with dissolution, and the overall conductivity of the alloy increases as observed in Figure 4.8.

With decreasing freezing rate, i.e. increasing DAS, the silicon particles become coarser (Fig. 4.13 b) whereas the degree of supersaturation of the matrix diminishes. Consequently, the rate of spheroidization drops while the diffusion process duration is longer during solution treatment. So, the effect of dissolution progressively outweighs that of spheroidization, and conductivity drops below its as cast level (Figure 4.8).

4.2 Modified Al-Si alloy

At 15 μm DAS, electrical conductivity is unchanged (Fig. 4.9) by solution treatment. Since dissolution in the almost saturated matrix is negligible, the transformation of fine silicon fibres into spheres is likely to have no effect on the conductivity of the alloy. Fibres and spheres therefore have the same effect with respect to electron scattering.

With increasing DAS, the dissolution process intensifies and conductivity progressively decreases since it is not affected by spheroidization.

The invariability of conductivity during artificial aging at 160°C is likely due to the non diffusion of silicon atoms in solid solution at this temperature as was mentioned before for the precipitation treatment.

4.3 Unmodified A356

As seen in Figure 4.11, the eutectic structure of the unmodified A356 alloy is coarser than that of the unmodified synthetic one. Besides, conductivity measurements on as cast samples have shown that fully unmodified alloys have a much lower conductivity than partially refined ones. Assuming that both structures have reached the same degree of spheroidization after solution treatment, electrical conductivity increase with spheroidization is consequently higher for A356 alloy than for synthetic. At higher DAS, spheroidization is not complete so that elongated silicon particles remain (Fig. 4.15) which impede the electron flow as do acicular plates. The effect of dissolution therefore prevails over that of spheroidization and the resulting electrical conductivity is lower than that in the as-cast state.

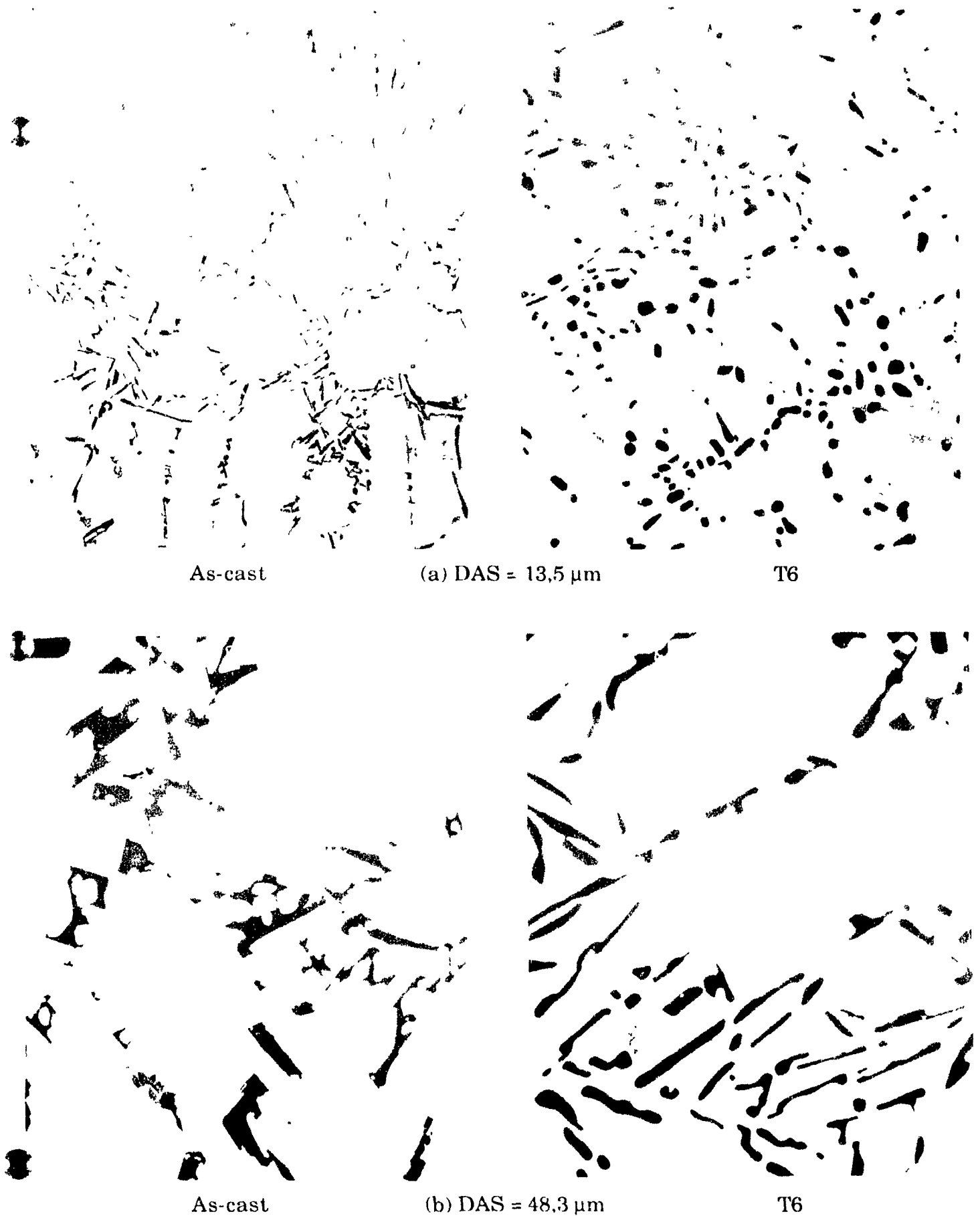


***Figure 4.15 : Micrographs of as cast and T6 unmodified A356 alloy
at two different DAS. Mag : X 500***

4.4 A356 modified alloy

The mechanism proposed to account for the observed decrease in conductivity of synthetic binary Al-Si alloys during heat treatment is also valid for A356 modified alloy.

4.5 Influence of precipitation

Conductivity does not vary significantly on artificial aging (Fig. 4.10 & 4.12) although a significant increase would be expected from theory. Mg Si precipitates are presumably very small and finely dispersed, thus conductivity remains almost unchanged. This hypothesis is supported by the fact that the optimum mechanical properties, which is what heat treatment aims at achieving, are obtained when the lattice strain by G.P. zones is a maximum, that is when conductivity is the lowest. To validate this assumption, some A356 step castings in T6 conditions were further treated at 200°C for 4 hours. The eddy current versus DAS plot obtained is shown on Figure 4.16 with the other plots drawn previously. It can be observed that the electrical conductivity has increased from 4 to 9 units of eddy current, but that in counterpart, the curve is almost flat which indicates that the correlation between conductivity and DAS has disappeared. This points out the importance of the artificial aging on the conductivity response to DAS changes which has to be precisely controlled. Unfortunately, in industrial practice, this level of precision is hardly obtained, and the conductivity method to predict DAS may become inoperative on T6 castings.

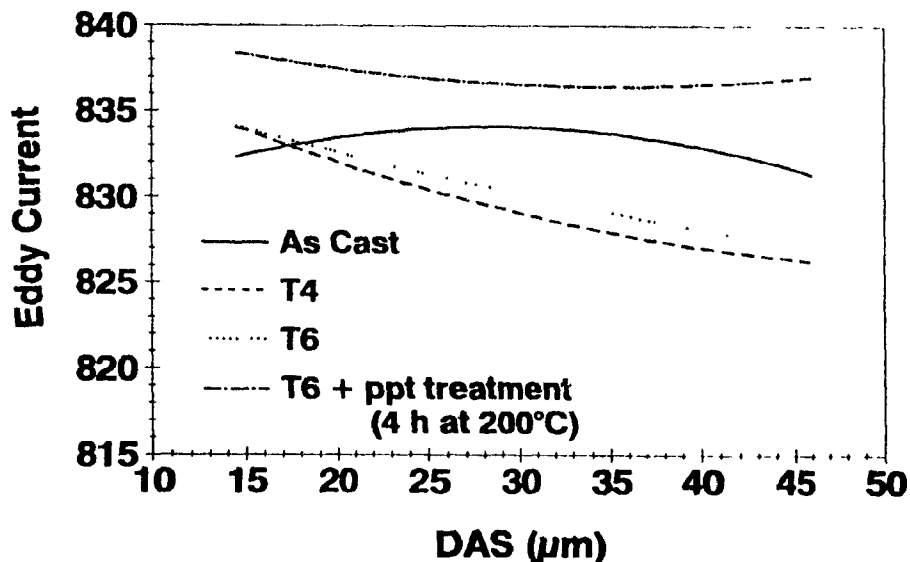


***Figure 4.16 : Conductivity vs DAS plots for A356 modified alloy.
Influence of overaging***

4.6 Potential Industrial Application

1 : In the as cast condition, the determination of DAS by conductivity measurement is difficult because of the importance of the effect of elements in solution on the electrical conductivity. In addition, the change in conductivity due to DAS, in the range of DAS covered, is about the same order as the difference of conductivity between a chilled and an unchilled sample having the same DAS.

This method is applicable to unchilled castings, but, in industrial practice, the areas of a casting where high mechanical properties are required, and therefore where knowing the DAS value is of interest for the metallurgist, are often heavily chilled.

- 2 : This method is probably best used immediately after quenching the casting in water (T4 condition) when the electrical conductivity DAS relationship is linear. In this condition, the variation of electrical conductivity with-DAS is 0.05 units of eddy current per micron (Figure 4.12), and, since the accuracy of the measurement is 2 units of eddy current, the error on the DAS prediction is 15 microns.

The accuracy of the method as presently configured is too low to consider its use in the foundry. However, if a new conductivity tester could be designed such that either the error on conductivity measurement would be reduced or the slope of the conductivity versus DAS curve increased, then the uncertainty on the DAS prediction could be reduced, and the method may gain interest for the foundryman.

In the T4 condition, time might be a factor to control since conductivity evolves as G.P. zone formation progresses [53].

- 3 : Although the electrical conductivity-DAS relationship is linear after artificial aging (T6 condition), the results obtained after an overaging treatment (Figure 4.16) have shown that electrical conductivity greatly depends on the type of artificial aging performed. In foundry practice, different artificial aging treatments are carried out on castings depending on the mechanical properties sought. Using the electrical conductivity technique on T6 castings would imply that conductivity versus DAS calibration curves have first been established for each artificial aging.

CONCLUSIONS

- 1- As cast conductivity decreases with increasing DAS in the range 30 μm to 50 μm . This effect is more pronounced for modified castings.
- 2- At lower DAS values ($<30 \mu\text{m}$), achieved by the use of a chill, precipitation in the solid state becomes important and its effect on electrical conductivity overcomes that of DAS.
- 3- The higher conductivity increase on chilled samples after precipitation treatment confirmed the effect of supersaturation of the aluminum matrix.
- 4- Modification is associated with a conductivity increase. The results of the present study confirm the possibility of predicting modification by electrical conductivity measurement
- 5- After solution treatment, conductivity versus DAS plots become linear as a result of the homogenisation of the aluminum matrix. But, the slopes of the curves are not important enough to predict DAS with an accuracy lower than 15 μm
- 6- For heat treated unmodified alloys, conductivity-DAS plots are affected by the differences in the degree of spheroidisation of the eutectic silicon plates.
- 7- Comparison of as cast and heat treated conductivities showed that a change from fibrous to spheroidised silicon has no effect on electrical conductivity.
- 8- Precipitation during artificial aging increases electrical conductivity and its effect is more important than that of DAS changes. The DAS measurement technique using electrical conductivity is best used immediately after quenching (T4 condition).

BIBLIOGRAPHY

- [1] L.F. Mondolfo, Aluminum alloys: Structure and Properties, Butterworth's & Co. Ltd., London, 1976
- [2] M. Garat, Hypoeutectic Al-Si alloys: Control of eutectic structure and mechanical properties, Aluminium, Alliages de Fonderie, Société de vente de l'Aluminium Pechiney, (technical brochures)
- [3] S. Bercovici, Control of solidification structures and properties of Al-Si alloys, Revue de l'Aluminium, pp. 85-89, Feb.(1979)
- [4] W.A Bailey, Foundry, pp 54-60, May (1964)
- [5] L. Bakerud, solidification characteristics of aluminium alloys - Vol 2 : foundry alloys - AFS/SKANALUMINIUM 1990
- [6] R. Guillot, L'Aluminium et ses alliages, Que sais-je ?, Presses Universitaires de France - n° 543-1984
- [7] A. Couture, AFS International Cast Metals Journal, 6, pp9-17 (1981)
- [8] Metals Handbook, Volume 15, 9th edition, American Society for Metals International, Metals Park, Ohio (1988)
- [9] Aluminium, Alliages de Fonderie, Société de Vente de l'Aluminium Pechiney (technical brochures)
- [10] Pacz, Aladar. U.S. Patent 1,387,900 (Aug. 16, 1921)
- [11] B. Closset and J.E. Gruzleski, Fonderie-Fondeur d'aujourd'hui, 16, pp.41-46 (1982)
- [12] C.W. Meyers and J.S. Chou, AFS Trans, 99, (1991), in press.
- [13] L. Grand, Revue de l'Aluminium, 29, pp.5-15, (1952)
- [14] W.R Opie and N.J. Grant, Trans AIME, 188, pp.1237-41 (1950)
- [15] L.E. Marsh and G. Reinemann, AFS Trans. 88, pp.413 (1979)
- [16] D. Argo, R.A.I. Drew and J.E. Gruzleski, AFS Trans., 95, pp. 455-64 (1987)

- [17] G.T. Meaden, Electrical Resistance of Metals, Phenom Press, New York, 1965, chapt. 3&5, pp. 59-82 & 110-123
- [18] F.R. Fickett, Cryogenics, vol 11, pp 349-367 (1971)
- [19] C.A. Wert & R M. Thomson, Physics of Solids, 2nd edition, Mc Graw-Hill, New York, 1970, pp. 227-239
- [20] J.M. Zimann, Electrons and Phonons, Oxford University Press, 1960, pp. 334-376
- [21] H.G. Van Bueren, Z. Metallkunde, vol 46, pp. 272-282 (1955)
- [22] L.V. Azaroff, Introduction to solids, Mc Graw-Hill, New York, 1960, chap. 2
- [23] C. Kittel, Introduction to solid state physics, J. Wiley & Sons, New York, 1956, Chap 10, pp. 234-310
- [24] L. Nordheim, Ann Physik, vol 9, pp. 607-640 (1931)
- [25] B.M Thall and B Chalmers, J Inst. Met., vol 77, pp. 79-97 (1950)
- [26] R. Iricibar, C. Pampillo and E.H. Chia, Aluminum Transformation Technology and Applications, ASM, Metals Park, OH, 1980 pp 241-303
- [27] J.E. Hatch, Aluminum Properties and Physical Metallurgy, ASM Int., Metals Park, OH, 1984
- [28] D.D. Pollock, Physical Properties of Materials for Engineers, CRC Press, Boca Raton, FL, 1982, Vol 2, Chap. 2, pp. 1-32
- [29] K. Schoder, Proc High Conductivity Copper and Aluminum Alloys, TMS AIME, pp 1-17 (1984)
- [30] G.K. Sigworth, AFS Trans vol 91, pp. 453-464 (1983)
- [31] G.K. Sigworth, S. Shivkumar and D Apelian, AFS Trans., vol 97, pp. 811-824, (1989)
- [32] R. Elliot, Eutectic Solidification Processing, Butterworths, London, 1983
- [33] L.M. Hogan and H. Sang, J. Cryst. Growth, vol 28, pp. 171-187 (1985)

- [34] H.A.H. Steen and A. Hellawell, *Acta Metall.*, 20, 363- 368 (1972)
- [35] P.B. Crosley and L.F. Mondolfo, *Modern Casting*, 1966, vol 49, pp. 53-64
- [36] S.Z. Lu and A Hellawell. *Prog. Mater Sci.*, 15, 1-12 (1970)
- [37] M.C. Flemings, Solidification Processing, Mater. Sci. and Eng. series, Mc Graw-Hill, 1974
- [38] I. Minkoff, Solidification and Cast Structures, J. Wiley & sons, 1986
- [39] K.F. Kobavashi and L.M. Hogan, *J. Mater. Sci.*, 20, pp. 1961-1978 (1985)
- [40] W. Kurz and D.J. Fisher, Fundamentals of Solidification, Trans. Tech. Publications, 1986
- [41] R.E. Spear and G.R Gardner, *AFS Trans.*, 71, pp. 209-215 (1963)
- [42] O. Vorren, J.E. Evensen and T.B. Pedersen, *AFS Trans.*, vol 92, pp. 459-466, (1984)
- [43] K.J. Oswalt and M.S. Misra, *AFS Trans*, vol 88, pp. 845-862, (1980)
- [44] S.F. Frederik and W.A. Bailey, *Trans Met. Soc. AIME*, 242, pp. 2063-2067 (1968)
- [45] W.A. Bailey, *Foundry*, 93, pp 96-98 (1965)
- [46] A. Scholin- Thesis- KTH Stockholm, Sweden, December 1982
- [47] W. Patterson and D. Amman, *Aluminium*, pp. 139-140 March 1959
- [48] K. Thirunavukkarasu and V. Panchanathan, *Aluminium*, 1978, vol 54, pp. 377-379
- [49] S. Jacob and A. Remy, *Fonderie-Fondeur d'aujourd'hui*, vol 22, pp. 33-41, (1983)
- [50] H. Oger, B. Closset and J.E. Gruzleski, *AFS Trans.*, vol 91, pp. 17-20 (1983)

- [51] B. Closset, K. Pirie and J.E. Gruzleski, AFS Trans., vol 92, pp. 123-133 (1984)
- [52] M.H. Mulazimoglu, R.A.L. Drew and J.E. Gruzleski, Met. Trans. A, vol 20A, . 383-389 (1989)
- [53] M.H. Mulazimoglu, PhD Thesis, McGill University, Montréal, Canada, 1988
- [54] P.S. Rosenbaum and D. Turnbull, Acta Metall., vol 6, pp. 653-659 (1958)
- [55] B. Closset, K. Pirie and J.E. Gruzleski, AFS Trans., vol 93, pp. 307-316, (1985)
- [56] R.A L Drew, B. Closset. and J.E. Gruzleski, AFS Trans., vol 94, pp. 9-16, (1986)
- [57] M.H. Mulazimoglu, R.A.L. Drew and J.E. Gruzleski, Canadian Metallurgical Quaterly, vol 28, pp. 251-258 (1989)
- [58] J.E. Gruzleski and B. Closset, The Treatment of Liquid Al-Si Alloys, AFS Inc, 1990, Chap 3, pp 52-53
- [59] La compacité des pièces en alliages légers - Actions des masselottes - Centre Technique des Industries de la Fonderie - 1972
- [60] T.J. Hurley, AFS Trans., vol 94, pp. 159-172, (1986)
- [61] G.K. Sigworth, Modern Casting, pp 23-25, July 1987
- [62] T.Z. Kattamis and M.C. Flemings, Trans AIME, 233-992 (1965)